

1 **Bacterial and eukaryotic intact polar lipids point to *in situ***
2 **production as a key source of labile organic matter in hadal**
3 **surface sediment of the Atacama Trench**

5 Edgارت Flores^{1,2,3*}, Sebastian I. Cantarero⁴, Paula Ruiz-Fernández^{1,2,3}, Nadia Dildar⁴,
6 Matthias Zabel⁵, Osvaldo Ulloa^{2,3} and Julio Sepúlveda^{3,4*}

8 ¹Programa de Postgrado en Oceanografía, Departamento de Oceanografía, Facultad de Ciencias Naturales y
9 Oceanográficas, Universidad de Concepción, Concepción, Chile

10 ²Departamento de Oceanografía, Universidad de Concepción, Casilla 160-C, Concepción, Chile

11 ³Millennium Institute of Oceanography, Universidad de Concepción, Concepción, Chile

12 ⁴Department of Geological Sciences and Institute of Arctic and Alpine Research, University of Colorado Boulder,
13 Boulder, CO 80309, USA

14 ⁵MARUM – Center for Marine Environmental Sciences & Department of Geosciences, Univ. of Bremen, D-
15 28334, Bremen, Germany

17 *Correspondence to: Edgارت Flores (edgart.flores@imo-chile.cl), Julio Sepúlveda (jsepulveda@colorado.edu)

19 **Abstract.** Elevated organic matter (OM) concentrations are found in hadal surface sediments relative to the
20 surrounding abyssal seabed. However, the origin of this biological material remains elusive. Here, we report on
21 the composition and distribution of cellular membrane intact polar lipids (IPLs) extracted from surface sediments
22 around the deepest points of the Atacama Trench and adjacent bathyal margin to assess and constrain the sources
23 of labile OM in the hadal seabed. Multiscale bootstrap resampling of IPLs' structural diversity and abundance
24 indicates distinct lipid signatures in the sediments of the Atacama Trench that are more closely related to those
25 found in bathyal sediments than to those previously reported for the upper ocean water column in the region.
26 Whereas the overall number of unique IPL structures in hadal sediments contributes a small fraction of the total
27 IPL pool, we also report a high contribution of phospholipids with mono- and di-unsaturated fatty acids that are
28 not associated with photoautotrophic sources, and that resemble traits of physiological adaptation to high pressure
29 and low temperature. Our results indicate that IPLs in hadal sediments of the Atacama Trench predominantly
30 derive from *in situ* microbial production and biomass, whereas the export of the most labile lipid component of
31 the OM pool from the euphotic zone and the overlying oxygen minimum zone is neglectable. While other OM
32 sources such as the downslope and/or lateral transport of labile OM cannot be ruled out and remain to be studied,
33 they are likely less important in view of the lability of ester-bond IPLs. Our results contribute to the understanding
34 of the mechanisms that control the delivery of labile OM to this extreme deep-sea ecosystem. Furthermore, they
35 provide insights into some potential physiological adaptation of the *in situ* microbial community to high pressure
36 and low temperature through lipid remodeling.

38 **1. Introduction**

39 The deep ocean has been classically considered a vast "biological desert" (Danovaro et al., 2003) due to the
40 attenuation of organic matter (OM) fluxes with increasing depth (Wakeham et al., 1984; Martin et al., 1987;
41 Hedges et al., 2001; Rex et al., 2006). However, hadal trenches (~6,000-11,000 m below sea level) contradict this
42 paradigm (Danovaro et al., 2003; Glud et al., 2013; Leduc et al., 2016; Wenzhöfer et al., 2016; Luo et al., 2017),

43 as they act as depocenters of OM (Jahnke and Jahnke, 2000) and hotspots for microbial activity (Glud et al., 2013;
44 Wenzhöfer et al., 2016; Liu et al., 2019). Indeed, OM availability is considered the major factor controlling the
45 abundance, biomass, and diversity of life in the deep ocean (Danovaro et al., 2003; Ichino et al., 2015), whereas
46 hydrostatic pressure appears to be an important and additional factor controlling biological activity in hadal trench
47 systems (Jamieson et al., 2010; Tamburini et al., 2013). However, our understanding of the composition, sources,
48 and lability of OM in marine trenches remains limited. According to Xu et al. (2018), the main sources of OM to
49 the hadal zone include: (1) the vertical sinking of particulate OM (POM); (2) the carrion falls of dead bodies; (3)
50 inputs of terrestrial OM; (4) downslope transport of OM from continental slopes; and (5) *in situ* chemosynthetic
51 production associated with cold seeps or hydrothermal vents. Several studies have highlighted the importance of
52 POM sinking mainly from the euphotic zone (Stockton and DeLaca, 1982; Angel, 1984; Gooday et al., 2010). In
53 fact, POM fluxes measured at 4,000 m in the North Pacific Subtropical Gyre Ocean reveal that a seasonal export
54 pulse can exceed the mean annual flux by ~150% (Poff et al., 2021). However, it is unknown whether such pulses
55 reach the hadal sediments (6,000-11,000 m). Downslope transport, on the other hand, can be facilitated by trench
56 topography and gravity (Jahnke et al., 1990; Fischer et al., 2009; Inthorn et al., 2006; Ichino et al., 2015) and/or
57 by earthquakes (Glud et al., 2013; Kioka et al., 2019), as recently reported in the Japan Trench (Schwestermann
58 et al., 2021). Independent of the main sources of OM, which are spatially and temporally variable, the channeling
59 of allochthonous OM to the hadal zone should be facilitated by the characteristic V-shape cross-section of
60 trenches, unique tectonic position in the ocean, and the physiography of the canyons that connect to coast systems
61 (Itou et al., 2000; Itoh et al., 2011; Bao et al., 2018). Additionally, autochthonous OM sources include *in situ*
62 microbial biomass production (Smith, 2012; Nunoura et al., 2016; Ta et al., 2019; Hand et al., 2020), although
63 their overall contribution as a secondary input to carbon budgets and energy flow in these systems remains poorly
64 constrained (Grabowski et al., 2019). The spatial variations in community structure seen in benthic prokaryotic
65 populations in hadal regions such as the Mariana, Japan, and Izu-Ogasawara trenches have been attributed to the
66 variability of biogeochemical conditions, mainly nitrate and oxygen availability (Hiraoka et al., 2020), with
67 benthic oxygen consumption exhibiting heterogeneity (Glud et al., 2021). Recent metagenomic data has revealed
68 the presence of abundant heterotrophic microorganisms in sediments of the Challenger Deep (Nunoura et al.,
69 2018), which are likely fueled by the endogenous recycling of available OM (Nunoura et al., 2015; Tarn et al.,
70 2016). Furthermore, the abundance of prokaryotes in hadal depths can be influenced by dynamic depositional
71 conditions (Schauberger et al., 2021), which in turn may be influenced by the intensity of propagating internal
72 tides (Turnewitsch et al., 2014). All these factors likely alter the deposition, distribution, and composition of OM
73 present in trench sediments.

74
75 An alternative approach to study microbial processes and the contribution of autochthonous OM is the use of cell
76 membrane intact polar lipids (IPLs), which although less specific than genomic markers, allow for more
77 quantitative estimates of microbial biomass in nature (e.g., Lipp et al., 2008; Schubotz et al., 2009; Cantarero et
78 al., 2020). IPLs are composed of a polar head group typically attached to a glycerol backbone from which aliphatic
79 chains are attached via ester and/or ether bonds (Sturt et al., 2004). Their structural diversity is given by the
80 modifications found in the different components of their chemical structure (e.g., polar head groups can be
81 comprised of phosphorous, nitrogen, sulfur, sugars, and amino acids), whereas aliphatic chains (alkyl or
82 isoprenoidal) can vary in their length (number of carbon atoms), and their degree of unsaturation, methylation,
83 hydroxylation, and cyclization (Van Mooy and Fredricks, 2010; Brandsma et al., 2011; Schubotz et al., 2013). In

84 bacteria and eukarya, alkyl chains are most commonly linked via an ester bond to the sn-glycerol-3-phosphate
85 backbone (Koga and Morii, 2007), although some bacteria are known to produce di- and tetraether lipids (Weijers
86 et al., 2007). The variability of membrane chemical structures underlies the adaptability of microbial lifestyles to
87 changing environmental conditions such as nutrients, temperature, oxygen, pH, and pressure (DeLong and
88 Yayanos, 1985; Somero, 1992; Van Mooy et al., 2009; Carini et al., 2015; Sebastián et al., 2016; Siliakus et al.,
89 2017; Boyer et al., 2020). Furthermore, since eukaryotic and bacterial ester-bond IPLs are more labile than ether-
90 bond counterparts (Logemann et al., 2011), they are suitable biomarkers to evaluate sources of labile OM in
91 marine environments.

92

93 IPLs have been previously used as microbial markers in diverse marine settings, such as along strong redox
94 gradients in the Black Sea (Schubotz et al., 2009b) and the oxygen minimum zones (OMZs) of the eastern tropical
95 Pacific (Schubotz et al., 2018a; Cantarero et al., 2020) and the Arabian Sea (Pitcher, 2011), as well as in surface
96 open ocean waters of the eastern south Pacific (Van Mooy and Fredricks, 2010), the northwestern Atlantic
97 (Popendorf et al., 2011b), and the Mediterranean Sea (Popendorf et al., 2011a), to name a few. Their utility as
98 markers of microbial diversity and processes has also been tested in marine sediments (Liu et al., 2011, 2012;
99 Sturt et al., 2004), such as along the Peru Margin, Equatorial Pacific, Hydrate Ridge, and Juan de Fuca Ridge
100 (Lipp and Hinrichs, 2009a) and in subsurface sediment layers from the Peru Margin (Biddle et al., 2006).
101 However, to the best of our knowledge, no IPL studies have been reported for sediments of hadal trenches.

102

103 In this study, we investigate the chemical diversity and abundance of microbial IPLs as markers of one the most
104 labile molecular fractions of OM in sediments of the deepest points of the Atacama Trench, and compare them to
105 IPL stocks in bathyal surface sediments (~500-1,200 m) and the overlying 700 m of the water column (Cantarero
106 et al., 2020). More specifically, we evaluate possible IPL provenance (*in situ* vs. allochthonous production), and
107 the presence of unique IPL signatures of the *in situ* microbial community as well as evidence for molecular
108 adaptations to the extreme conditions of the hadal region.

109

110 **2. Material and Methods**

111

112 **2.1 Study areas and sampling**

113

114 The Atacama Trench is located in the eastern tropical South Pacific (ETSP) along the Peru-Chile margin, and it
115 underlies the eutrophic and highly productive Humboldt Current System (Angel, 1982; Ahumada, 1989), which
116 includes the fourth largest (by volume) oxygen minimum zone (OMZ) in the world (Schneider et al., 2006). In
117 this area, while there is minimal river runoff (Houston, 2006), winds can transfer dust from the adjacent
118 continental desert (Angel, 1982). With an extension of ~5,900 km, the Atacama Trench is the world's largest
119 trench (Sabbatini et al., 2002), whereas it is geographically isolated from other trenches in the Pacific Ocean.

120

121 In this study, we investigated the diversity and abundance of bacterial and eukaryotic IPLs in a total of 9 hadal
122 surface (0-1 cm) and subsurface (1-2 and 2-3 cm) sediments (3 sites between 7,734 and 8,063 m water depth)
123 collected during the HADES-SO261 cruise (March to April 2018) onboard the RV *Sonne* (Wenzhöfer, 2019), and
124 7 bathyal surface sediments (7 sites; 529-1200 m water depth) collected during the ChiMeBo-SO211 cruise

125 (November 2-29, 2010) onboard the RV *Sonne* (Matys et al., 2017) (Table 1; Fig. 1). We compare our results
 126 against IPL results from the overlying water column (0-700 m) recently reported in Cantarero et al. (2020).

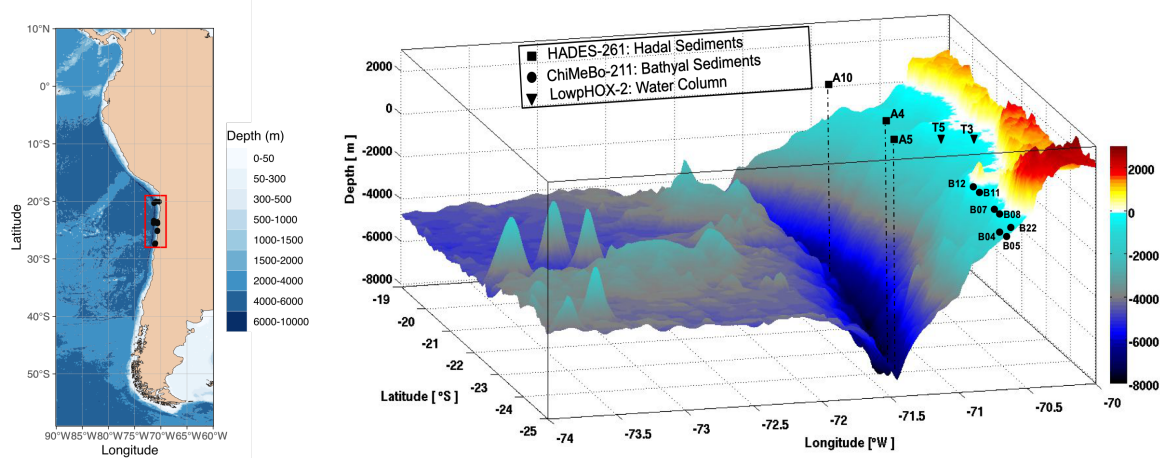
127

128 **Table 1. Sampling stations from the Hades, ChiMeBo, and LowpHOX-2 expeditions.**

129

Cruise-RV	Device	Environment	Station	Environmental samples	Sampling depth (m)	Latitude (°S)	Longitude (°W)	Date	Reference
HADES SONNE SO-261	Multi-corer (MUC)	Hadal sediments	A10	Hadal sediments (0-1, 1-2 and 2-3 cm)	7734	20.32	71.29	26/03/2018	
			A5	Hadal sediments (0-1, 1-2 and 2-3 cm)	7890	23.81	71.37	11/03/2018	
			A4	Hadal sediments (0-1, 1-2 and 2-3 cm)	8063	23.36	71.34	14/03/2018	
ChiMeBo SONNE SO-211	Multi-corer (MUC)	Bathyal Sediments	B12	Upper bathyal sediment (0-1 cm)	529	23.59	70.67	02-29/11/2010	
			B08	Upper bathyal sediment (0-1 cm)	539	25.2	70.68	02-29/11/2010	
			B22	Upper bathyal sediment (0-1 cm)	545	27.29	71.05	02-29/11/2010	
			B07	Lower bathyal sediment (0-1 cm)	920	25.07	70.66	02-29/11/2010	This study
			B05	Lower bathyal sediment (0-1 cm)	957	27.5	71.13	02-29/11/2010	
			B11	Lower bathyal sediment (0-1 cm)	1113	23.85	70.65	02-29/11/2010	
			B04	Lower bathyal sediment (0-1 cm)	1200	27.45	71.16	02-29/11/2010	
LowpHOX-2 Cabo de Hornos	Rosette (Niskin bottles)	Water column	T3/T5	Chlorophyll maximum (0.3-2.7 μ m)	9-10	20.07/20.03	70.36/70.89	04-06/02/2018	
			T3/T5	Upper chemocline (0.3-2.7 μ m)	25-28	20.07/20.03	70.36/70.89	04-06/02/2018	
			T3/T5	Lower chemocline (0.3-2.7 μ m)	35-45	20.07/20.03	70.36/70.89	04-06/02/2018	Cantarero et al., 2020
			T3/T5	Upper OMZ (0.3-2.7 μ m)	55-60	20.07/20.03	70.36/70.89	04-06/02/2018	
			T3/T5	Core OMZ (0.3-2.7 μ m)	250	20.07/20.03	70.36/70.89	04-06/02/2018	
			T3/T5	Mesopelagic zone (0.3-2.7 μ m)	750	20.07/20.03	70.36/70.89	04-06/02/2018	

130
 131
 132



133

134 **Figure 1. Three-dimensional map of the Atacama Trench showing the sampling locations of this study. The black**
 135 **squares indicate the hadal sediment sampling stations, the black circles indicate the bathyal sediment sampling stations**
 136 **from Matys et al. (2017), and the black triangles indicate water column sampling stations from Cantarero et al. (2020).**

137

138

139

140

141 Sediment samples were collected using a multi-corer (MUC) equipped with twelve 60-cm-long acrylic tubes (6-
 142 10 cm diameter for bathyal sediments and 9.5 cm diameter for hadal sediments). During the HADES expedition,
 143 an autonomous lander equipped with a Seabird SBE-19 plus CTD and 2 Niskin bottles (30 L) was used to obtain
 144 hydrographic data down to ~7850 m. Hadal sediments from the HADES-SO261 cruise were stored at 4°C until
 145 they were extruded and subsampled onboard at 1-cm resolution, and then kept frozen at -20°C until their
 146 processing in the laboratory. Further information about sample collection of bathyal and hadal sediments during
 147 the ChiMeBo-SO211 and HADES-SO261 cruises can be found in Matys et al. (2017) and Wenzhöfer et al.,
 148 respectively.

149 We compare our IPL results from surface sediment in the hadal and bathyal regions against samples from the
150 overlying water column from the LowPhOx-2 cruise recently reported by Cantarero et al. (2020). This includes
151 size-fractionated suspended OM (0.3-2.7 μ m and 2.7-53 μ m) at two stations and from six water depths that are
152 representative of the dominant biogeochemical zonation associated with the OMZ of this region: chlorophyll
153 maximum (~10 m), upper chemocline (~25 m), lower chemocline (~45 m), upper OMZ (~60 m), core OMZ (~250
154 m), and mesopelagic zone (~750 m) (See Table 1 and Cantarero et al., 2020 for further details).

155

156 **2.2 Analytical methods**

157

158 **2.2.1 Lipid extraction**

159

160 All samples were processed, extracted, and analyzed in the Organic Geochemistry Laboratory at the University
161 of Colorado Boulder. Sediment samples were freeze dried before extraction. Approximately 1-2 grams of dry
162 sediment was placed in a combusted glass centrifuge tube and extracted using a modified version (Wörmer et al.,
163 2013) of the Bligh and Dyer Extraction method (Bligh and Dyer, 1959) as detailed in Cantarero et al. (2020).
164 Briefly, before extraction, we added 1 μ g of C16 PAF ($C_{26}H_{54}NO_7P$) to each sample as an internal standard.
165 Samples were sequentially extracted using dichloromethane:MeOH:phosphate buffer (1:2:0.8 v:v:v; 2x),
166 dichloromethane:MeOH:trichloroacetic buffer (1:2:0.8 v:v:v; 2x) and dichloromethane:MeOH (1:5 v:v; 1x). After
167 each addition, samples were vortexed for 30 seconds, sonicated for 10 minutes, and then centrifuged for 5 minutes
168 at 2000 rpm. Each extraction was then transferred to a separatory funnel where a total lipid extract (TLE) was
169 combined and then concentrated under a gentle N_2 stream. Before analysis, the TLEs were resuspended in
170 dichloromethane:methanol (9:1) v/v and filtered through a 0.45 μ m polytetrafluoroethylene (PTFE) syringe filter.
171 The processing and extraction of bathyal sediments from the ChiMeBo-SO211 cruise and water column samples
172 from the LowpHOx-2 cruise has been reported by Matys et al. (2017) and Cantarero et al. (2020), respectively.
173 TLEs were transferred into 2 ml vials with 200 μ l inserts, and dissolved in 100 μ l of dichloromethane:MeOH [9:1,
174 v:v].

175

176 **2.2.2 IPL analysis**

177

178 IPL were analyzed according to Wörmer et al. (2013) and as described in Cantarero et al. (2020) using a Thermo
179 Scientific Ultimate 3000 High Performance Liquid Chromatograph (HPLC) coupled to a Q Exactive Focus
180 Orbitrap-Quadrupole High Resolution Mass Spectrometer (HPLC-HRMS) via electrospray ionization (ESI). The
181 HPLC program comprised a flow rate of 0.4 mL/min using a mixture of two mobile phases: mixture A consisted
182 of acetonitrile:dichloromethane (75:25, v:v) with 0.01% formic acid and 0.01% NH_4OH ; mixture B consisted of
183 methanol:water (50:50, v:v) with 0.4% formic acid and 0.4% NH_4OH . We used a linear gradient as follows: 1%
184 B (0–2.5 min), 5% (4 min), 25% B (22.5 min), 40% B (26.5 min–27.5 min), and the HPLC column was kept at
185 40 °C. Samples were injected (10 μ l) dissolved in dichloromethane:methanol (9:1, v:v). IPLs were separated using
186 a Waters Acuity BEH Amide column (2.1 \times 150 mm; 1.7 μ m particle size) that enables class-specific separation
187 based on their hydrophilic head group (Wörmer et al., 2013).

188

189 ESI settings comprised: sheath gas (N₂) pressure 35 (arbitrary units), auxiliary gas (N₂) pressure 13 (arbitrary
190 units), spray voltage 3.5 kV (positive ion ESI), capillary temperature 265°C, S-Lens RF level 55 (arbitrary units).
191 The instrument was calibrated for mass resolution and accuracy using the Thermo Scientific Pierce LTQ Velos
192 ESI Positive Ion Calibration Solution (containing a mixture of caffeine, MRFA, Ultramark 1621, and N-
193 butylamine in an acetonitrile/methanol/acetic acid solution).

194
195 IPLs were identified on positive ionization mode, on both full scan and data depended MS², based on their
196 molecular weights as either protonated (M + H)⁺ or ammonium (M + NH₄)⁺ adducts compounds, fragmentation
197 patterns, and retention times, and as compared against relevant literature (Sturt et al., 2004; Schubotz et al., 2009a;
198 Wakeham et al., 2012) and the internal database of the Organic Geochemistry Lab at CU Boulder.

199
200 The peak areas of individual IPLs were integrated using the Thermo Fisher Scientific TraceFinder software using
201 extracted ion chromatograms of their characteristic molecular ions. IPL abundances were determined with a
202 combination of an internal standard (C₁₆PAF, Avanti Lipids) and an external calibration to a linear regression
203 between peak areas and known concentrations of an IPL cocktail comprised of 17 different IPL classes across a
204 5-point dilution series (0.001–2.5 ng/μl) (see Cantarero et al., 2020). Deuterated standards (Avanti Lipids: d7-PC,
205 d7-PG, d7-PE and d9-DGTS) were used to correct for potential matrix effects on ionization efficiency. Despite
206 the limited number of available deuterated standards, on average, we observed that the matrix effect accounts for
207 a loss of ~7±0.6% in ionization efficiency. Therefore, it is reasonable to assume a similar loss for other IPL classes,
208 although this remains to be tested in future studies. We highlight the importance of using as many IPLs classes as
209 possible to account for both differences in ionization efficiency and matrix effect when performing IPL
210 quantification in environmental samples. The relative response factors followed the order: MGDG
211 >DGTS>DGTA >PDME >PME >PG > PC> PE >SQDG > DGCC > DGDG. Lipids classes were grouped into
212 phospholipids (PG; phosphatidylglycerol, PE; phosphatidylethanolamine, PC; phosphatidylcholine, and
213 PME/PDME; Phosphatidyl(di)methylethanolamine), glycolipids (MG; Monoglycosyldiacylglycerol, DG;
214 Diglycosyldiacylglycerol, and SQDG; Sulfoquinovosyldiacylglycerol), Betaine lipids (DGTA; Diacylglyceryl
215 hydroxymethyl-trimethyl-β-alanine, DGTS; Diacylglyceryl trimethylhomoserine, and DGCC;
216 Diacylglycerylcarboxy-N-hydroxymethyl-choline) and Other lipids (Gly-Cer; Glycosidic ceramides, PI;
217 phosphatidylinositol, and OL; Ornithine lipids). In addition, we use DAG to designate a diacylglycerol and AEG
218 to designate an acyletherglycerol, and we describe short- and long-chains to refer to combined alkyl chains of C₂₈-
219 and C₃₆₋₄₄, respectively (Rêzanka et al., 2009; Schubotz et al., 2009a; Brandsma., et al., 2011).

220
221

222 **2.3 Statistical analyses**

223
224 We used the Bray–Curtis similarity coefficient (Mirzaei et al., 2008) to produce hierarchical clustering of the
225 abundance of classes and molecules of IPLs, two types of p-values were available: approximately unbiased (AU)
226 p-value and bootstrap probability (BP) value with the number of bootstrap replications of 10,000 (Suzuki and
227 Shimodaira, 2006). We performed non-metric Multidimensional Scaling (NMDS) (Warton et al., 2012) to
228 examine the dissimilarity between the IPLs in each sample. The calculated distances to group centroids were based
229 on Bray-Curtis dissimilarity from IPLs abundances matrix, and the significance of the associations was determined

230 by 999 random permutations. Significance tests of the multivariate dissimilarity between groups were made using
231 Analysis of Similarity (ANOSIM), where complete separation and no separation among groups is suggested by R
232 = 1 and R = 0, respectively (Clarke and Gorley, 2015). Statistical differences in the numbers of carbon atoms and
233 double bonds were identified by ANOVA and Tukey's HSD (honestly significant difference) post hoc test. We
234 used similarity of percentage (SIMPER) analysis to identify the percentage contributions of IPLs which accounted
235 for > 90% of the similarity within each cluster. The multivariate statistical analyzes, as well as other statistical
236 analyses were calculated using the Vegan package (Oksanen et al., 2013) of open-source software R version 3.6.2
237 within the ggplots package (Warnes et al., 2015).

238

239 **3. Results**

240

241 **3.1 Hydrographic conditions**

242

243 A physical-chemical characterization of the water column during the ChiMeBo-SO211, LowpHOx-2, and
244 HADES-SO261 cruises has been reported in Matys et al. (2017), Cantarero et al. (2020) and Vargas et al. (2021),
245 and Fernández-Urruzola et al. (2021), respectively. Briefly, the potential temperature-salinity-dissolved oxygen
246 (θ -s-O₂) diagrams revealed an oxygenated and well-mixed water mass occupying the deeper parts of the Atacama
247 Trench (Fig. S1). However, the upper 1000 m shows variability in temperature (12-23 °C), salinity (34.4-34.8
248 psu) and oxygen (0.5-267 µM). More stable physical-chemical conditions are apparent in the mesopelagic and
249 bathypelagic zone of the Atacama Trench between 1000 and 4000 m, (temperature ~ 2.3 °C, salinity ~34.6 psu,
250 oxygen ~120.6 µM). Below 4000 m, average conditions were characterized by a potential temperature ~1.8 °C,
251 salinity ~34.7 psu, and oxygen ~143 µM (Fig. S1).

252

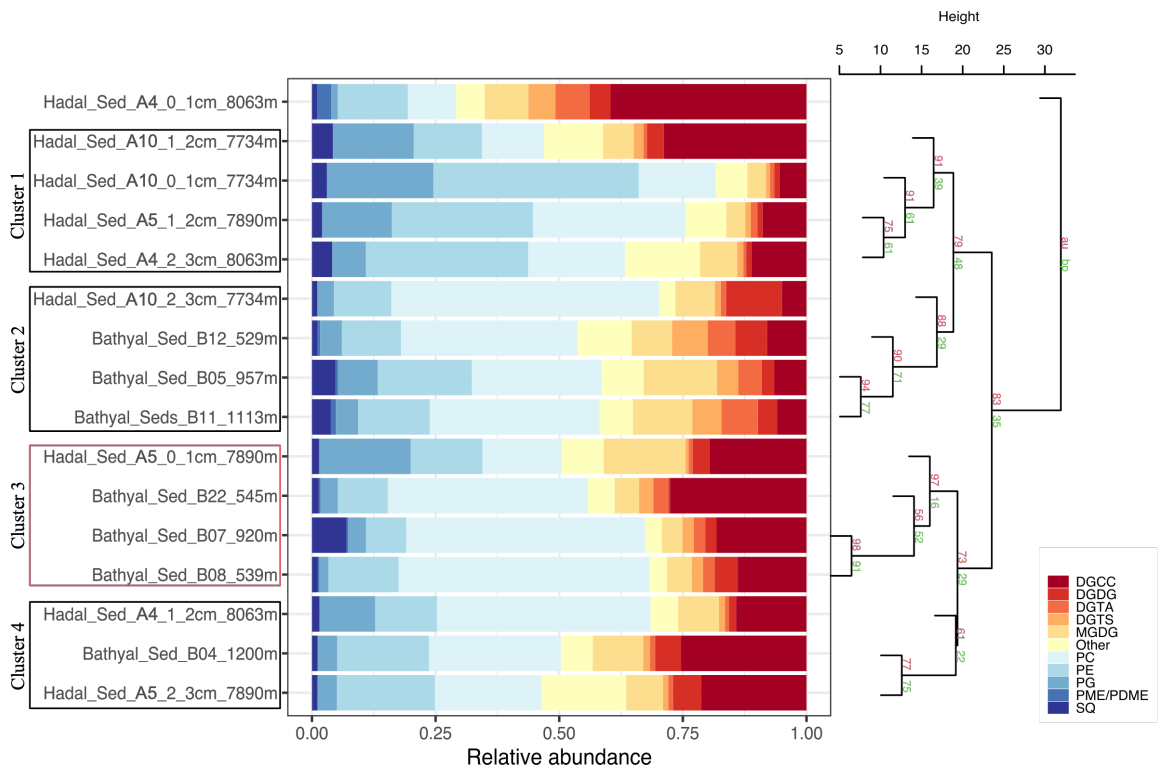
253 **3.2 IPLs in surface sediments of the Atacama trench**

254

255 **3.2.1 Distribution of IPL classes by polar head groups**

256

257 The 16 sediment samples from bathyal and hadal regions statistically grouped into four clusters based on their
258 dominant polar head group classes (Fig. 2, chemical structures in Fig. S2). Clusters 1 and 2 had approximately
259 unbiased (AU) p-values of 91% and 88%, respectively. Cluster 3 had the highest AU p-value of ≥ 97%, whereas
260 Cluster 4 had the lowest AU p-value of 61%. The cluster analysis revealed a degree of spatial heterogeneity
261 between bathyal and hadal depths and between the top three centimeters of hadal sediments, which results in the
262 lack of a clear separation between hadal and bathyal environments. In addition, the 0-1 cm hadal sediments at A4
263 station were un-clustered, consistent with a distinct distribution pattern of IPL classes. Cluster 1, composed of
264 only hadal samples from three different stations and depths, included phospholipids as the most abundant IPL
265 class (Fig. 2). Clusters 2, 3 and 4, composed of mixed bathyal and hadal samples, were mostly differentiated by
266 changes in the relative abundances of non-phosphorous IPLs including betaine classes. The un-clustered sample
267 was characterized by the lowest relative abundance of phospholipids and the highest relative abundance of betaine
268 lipids (especially DGCC).

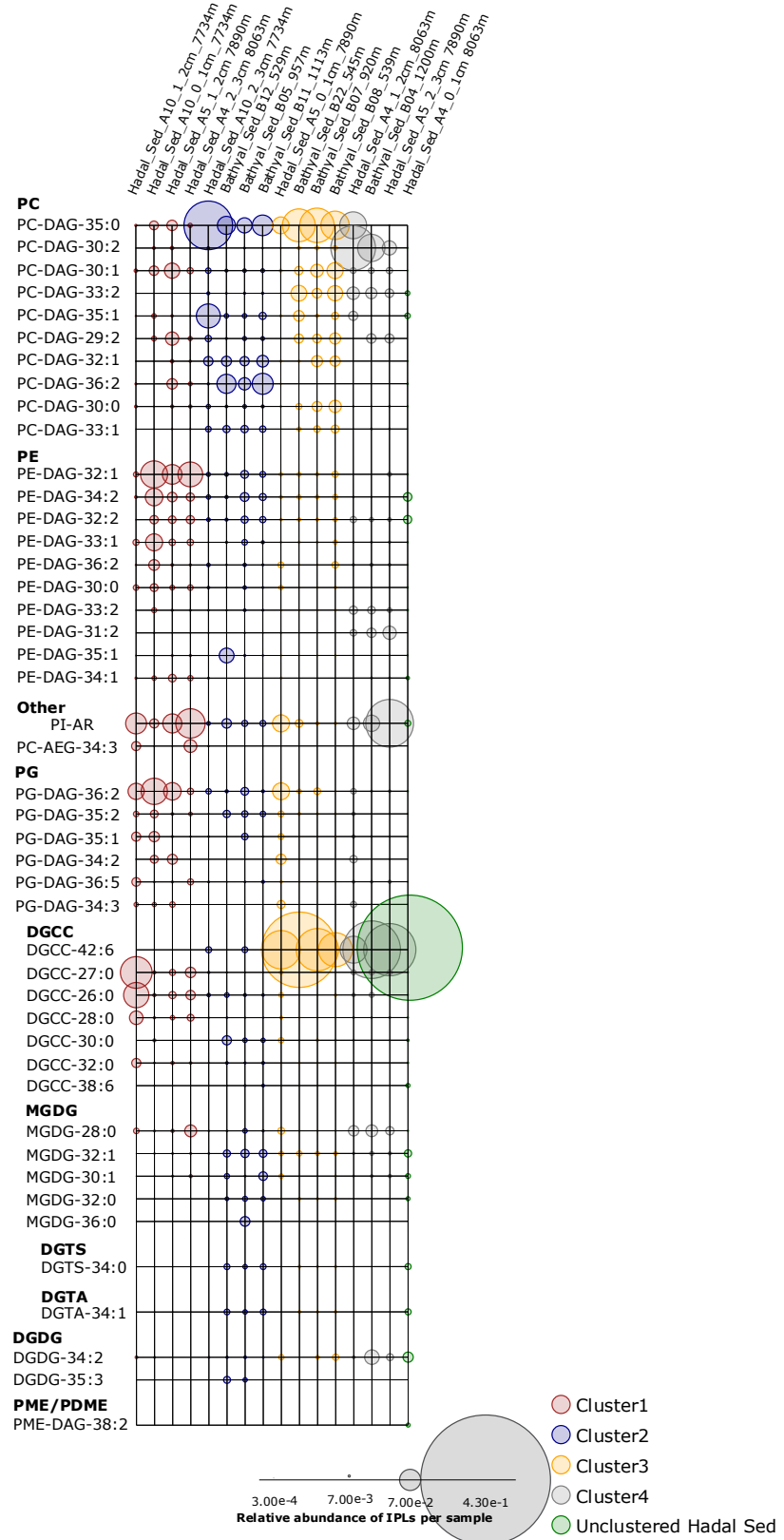


269
270 **Figure 2. Cumulative bar charts of the fractional abundance of IPL classes in each surface sediment sample from the**
271 **bathyal and hadal regions (left panel). Samples were grouped according to arithmetic mean (UPGMA) hierarchical**
272 **clustering based on Euclidean distances. The p-values are shown at branches, with AU in red and BP in green (right**
273 **panel). Clusters 3 with an AU $\geq 95\%$ confidence are indicated by the red rectangles (left) and are considered to be**
274 **strongly supported by the data.**

275 3.2.2 Distribution of individual IPLs

276
277 An overview of the most important IPLs contributing to dissimilarity between samples was obtained through a
278 SIMPER analysis based on Bray-Curtis coefficient within each cluster (Fig. 3). Samples in Cluster 1 were on
279 average 59.5% similar, with 14 individual IPLs contributing 50.6% of the total similarity. This cluster exhibited
280 a high contribution of PE-DAG (32:1, 33:1, and 34:2), PG-DAG (36:2), and DGCC (26:0, 27:0 and 28:0)
281 molecules (Table 2). Additionally, this cluster exhibited a large diversity of PC molecules, although with a low
282 relative abundance (Fig. 3). Samples in Cluster 2, on the other hand, which includes mainly bathyal stations, were
283 on average 58.8% similar and exhibited a high contribution of PC-DAG (35:0, 32:1, 36:2, 33:1, and 35:1) (Table
284 2). While this cluster shows a wide range of molecules, including PG, PE and MGDG, their relative contributions
285 are low (Fig. 3). Samples in Cluster 3 were on average 57.3% similar and included three bathyal and one hadal
286 stations. This cluster exhibited a high contribution of DGCC (42:6) and PC-DAG (35:0, 33:2, 30:1, and 29:2)
287 molecules (Table 2). Samples in Cluster 4 were on average 63.6% similar, and exhibited a high contribution of
288 PC-DAG (30:2, 33:2), DGCC (42:6), MGDG (28:0), and PE-DAG (33:2 and 31:2) molecules (Table 2). The un-
289 cluster sample (Hadal sediment of 0-1 cm at A4 station) is mainly composed by the DGCC 42:6 (Fig. 3). In
290 general, phospholipids showed a wide distribution and were found across all sediment samples. The total
291 dissimilarity between Clusters 1 and 2 was 59.17%, with PC-DAG-35:0, PE-DAG-32:1, PI-AR, PG-DAG-36:2,
292 DGCC 27:0, PC-DAG-36:2, PC-DAG-34:1, PC-DAG-32:1, DGCC 26:0, and PC-DAG-35:1 contributing 32.4%
293 of it (Table 2). The total dissimilarity between Clusters 1 and 3 was 60.7%, with DGCC 42:6, PC-DAG-35:0, PI-
294

296 AR, PE 32:1, PG-DAG-36:2, DGCC 27:0 and 26:0, and PC-DAG-33:2 contributing 38.1% of it (Table 2). The
 297 total dissimilarity between Clusters 1 and 4 was 62.5%, with DGCC 42:6, PC-DAG-30:2, PE 32:1, PC-DAG-
 298 35:0, PG-DAG-36:2, PC-DAG-33:2, and DGCC 27:0 contributing 37.62% of it (Table 2).



300
301
302
303
304
305
306
307

Figure 3. Relative abundance of individual IPLs contributing most of the dissimilarity between the 4 clusters shown in Fig. 2. Sampling stations are organized left to right and are shown using the same order from hierarchical clusters in Fig. 2, whereas IPL classes are organized from top to bottom. The circle size is proportional to the relative abundance of IPLs in each sample (bottom panel).

Table 2. Similarity percentage (SIMPER) analysis. The average abundance and contribution of IPLs that explain the main differences among the sediment samples is based on the hierarchical clusters shown in Fig. 2.

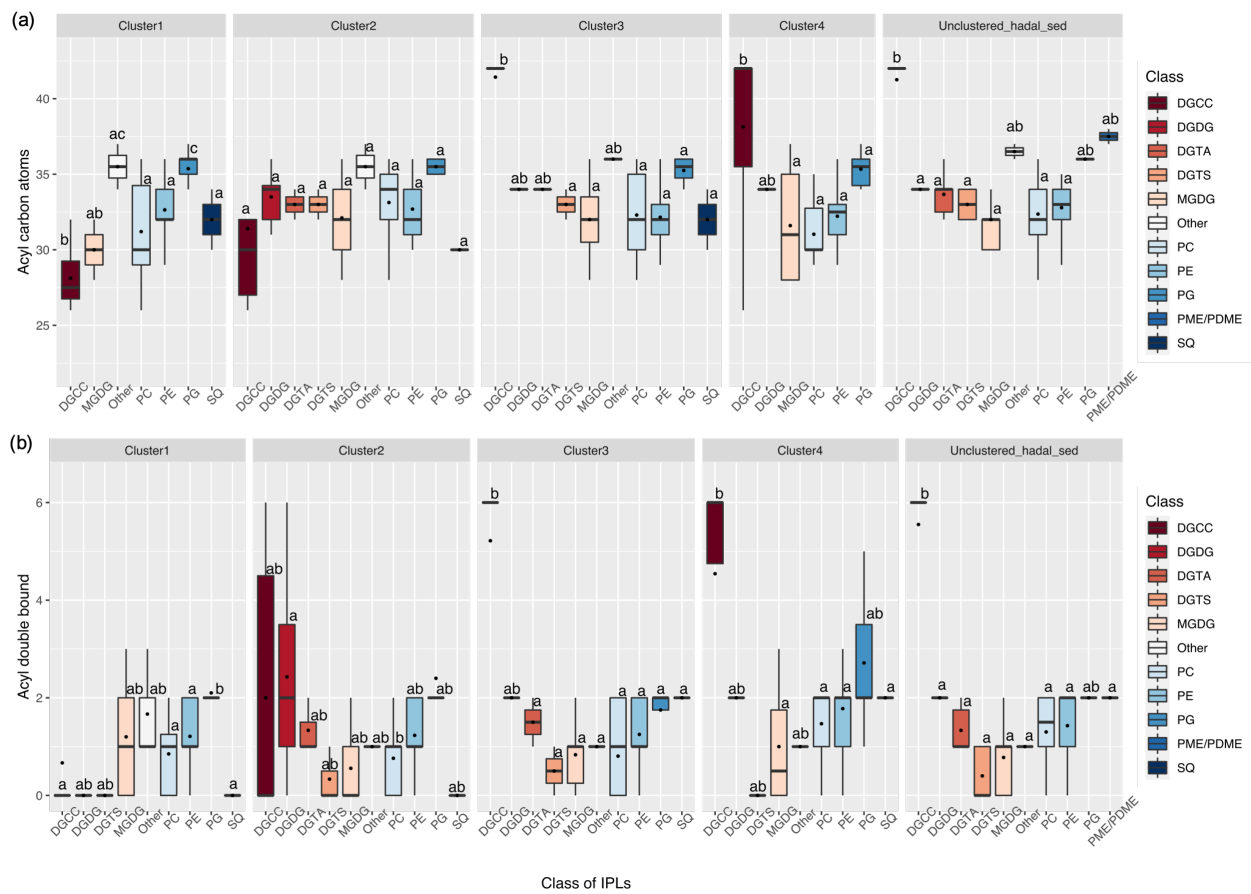
Group Cluster 1						Groups Cluster 1 & Cluster 2					
Cluster 1: Average Similarity = 59.53						Average dissimilarity = 59.17					
IPLs	Average Cluster 1	Average Similarity	Similarity/S	Contribution (%)	Cumulative (%)	IPLs	Average Cluster 1	Average Cluster 2	Dissimilarity y/SD	Contribution (%)	Cumulative (%)
PI-AR	0.06	4.76	2.46	7.99	7.99	PC-DAG-35:0	0.02	0.08	3.18	1.34	5.37
PE-DAG-32:1	0.06	4.37	1.45	7.34	15.33	PE-DAG-32:1	0.06	0.02	2.35	1.73	9.35
PG-DAG-36:2	0.05	3.79	2	6.36	21.69	PI-AR	0.06	0.02	2.21	1.74	3.73
PE-DAG-33:1	0.03	2.06	33.49	3.45	25.14	PG-DAG-36:2	0.05	0.02	1.98	1.64	16.43
PE-DAG-34:2	0.03	1.89	1.74	3.17	28.31	DGCC-27:0	0.04	0	1.93	1	3.26
DGCC-26:0	0.04	1.84	2.04	3.09	31.4	PC-DAG-36:2	0.01	0.05	1.79	1.57	22.71
PC-DAG-30:1	0.03	1.76	2.21	2.96	34.36	PC-DAG-34:1	0	0.04	1.79	1.03	3.02
DGCC-27:0	0.04	1.74	1.8	2.93	37.3	PC-DAG-32:1	0.01	0.03	1.36	5.58	28.03
PE-DAG-30:0	0.02	1.7	13.1	2.86	40.15	DGCC-26:0	0.04	0.01	1.34	0.95	30.3
PE-DAG-32:2	0.02	1.39	1.07	2.34	42.49	PC-DAG-35:1	0.01	0.03	1.27	0.9	32.45
PC-DAG-35:0	0.02	1.31	1.52	2.2	44.69	PE-DAG-33:1	0.03	0.01	1.02	1.2	34.18
DGCC-28:0	0.02	1.22	1.96	2.05	46.74	PC-DAG-33:1	0	0.02	0.96	7.61	35.8
PC-DAG-26:0	0.02	1.18	1.46	1.99	48.73	DGCC-28:0	0.02	0	0.93	1.28	37.37
PC-DAG-28:0	0.02	1.14	1.59	1.91	50.63	PC-AEG-34:3	0.02	0	0.9	1.03	38.89
Group Cluster 2						PC-DAG-34:2	0.03	0.02	0.88	1.2	40.38
Cluster 2: Average Similarity = 58.79						MGDG-32:1	0	0.02	0.83	1.81	41.78
IPLs	Average Cluster 2	Average Similarity	Similarity/S	Contribution (%)	Cumulative (%)	PC-DAG-30:1	0.03	0.01	0.83	1.15	43.18
PC-DAG-35:0	0.08	5.63	7.54	9.58	9.58	PG-DAG-34:2	0.02	0	0.77	1.05	44.48
PC-DAG-32:1	0.03	3.12	31.24	5.3	14.88	PE-DAG-33:0	0.02	0	0.76	1.11	45.77
PC-DAG-36:2	0.05	2.74	1.13	4.67	19.55	PG-DAG-35:1	0.02	0.01	0.74	1.22	47.03
PC-DAG-33:1	0.02	2.04	10.17	3.46	23.01	PE-DAG-34:1	0.02	0	0.74	2.06	48.27
PC-DAG-35:1	0.03	1.63	4.48	2.77	25.78	PC-DAG-26:0	0.02	0	0.72	1.74	49.48
PI-AR	0.02	1.61	3.9	2.74	28.53	DGCC-30:0	0	0.01	0.68	1.32	50.64
MGDG-32:1	0.02	1.44	1.35	2.45	30.98	Groups Cluster 1 & Cluster 3					
PE-DAG-32:1	0.02	1.38	5.03	2.35	33.33	Average dissimilarity = 60.69					
PE-DAG-34:2	0.02	1.38	2.75	2.35	35.68	IPLs					
PE-DAG-32:2	0.02	1.22	2.79	2.08	37.76	DGCC-42:6	0	0.16	8.02	3.2	13.21
PC-DAG-32:0	0.01	1.14	5.69	1.94	39.69	PC-DAG-35:0	0.02	0.08	3.05	1.87	18.23
PG-DAG-36:2	0.02	1.1	3.23	1.87	41.57	PI-AR	0.06	0.05	2.66	1.6	22.62
PG-DAG-35:2	0.02	1.09	1.23	1.86	43.43	PE-DAG-32:1	0.06	0.01	2.49	1.74	26.72
PC-DAG-34:1	0.04	1.06	0.41	1.8	45.23	PG-DAG-36:2	0.05	0.02	1.9	1.49	29.86
PC-DAG-30:1	0.01	1.05	7.23	1.79	47.02	DGCC-27:0	0.04	0.01	1.84	0.97	30.3
PC-DAG-32:2	0.01	0.95	11.7	1.61	48.64	DGCC-26:0	0.04	0.01	1.59	1.12	35.52
PC-DAG-29:2	0.01	0.95	1.79	1.2	40.89	PC-DAG-33:2	0	0.03	1.58	1.7	38.12
PC-DAG-29:2	0.01	0.95	2.69	1.61	50.25	PE-DAG-34:2	0.03	0.01	1.13	1.35	39.98
Group Cluster 3						PE-DAG-33:1	0.03	0.01	1.07	1.33	41.75
Cluster 3: Average Similarity = 57.31						PC-AEG-34:3	0.02	0	0.95	1.08	43.31
IPLs	Average Cluster 3	Average Similarity	Similarity/S	Contribution (%)	Cumulative (%)	PC-DAG-29:2	0.02	0.03	0.95	1.88	44.87
DGCC-42:6	0.16	12.84	6.72	22.4	22.4	DGCC-28:0	0.02	0	0.9	1.25	46.36
PC-DAG-35:0	0.08	4.78	1.14	8.33	30.74	PC-DAG-30:1	0.03	0.03	0.87	1.35	47.79
PC-DAG-33:2	0.03	2.07	1.19	3.61	34.35	PE-DAG-33:0	0.02	0	0.76	1.07	1.26
PC-DAG-30:1	0.03	1.96	1.82	3.42	37.77	PE-DAG-34:2	0.02	0.01	0.76	1.1	50.3
PC-DAG-29:2	0.03	1.79	1.2	3.12	40.89	Groups Cluster 1 & Cluster 4					
PI-AR	0.05	1.69	1.09	2.95	43.84	Average dissimilarity = 62.47					
MGDG-32:1	0.01	1.22	7.66	2.14	45.98	IPLs					
PE-DAG-32:1	0.01	1.18	10.45	2.05	48.03	DGCC-42:6	0	0.14	6.99	2.57	11.19
PC-DAG-30:0	0.02	1.13	1.22	1.97	50	PC-DAG-30:2	0.01	0.12	5.66	3.64	20.24
Group Cluster 4						PE-DAG-32:1	0.06	0	3.17	2.09	25.31
Cluster 4: Average Similarity = 63.64						PC-DAG-35:0	0.02	0.04	2.22	1.6	3.55
IPLs	Average Cluster 2	Average Similarity	Similarity/S	Contribution (%)	Cumulative (%)	PG-DAG-36:2	0.05	0.01	2.12	1.64	32.27
PC-DAG-30:2	0.12	9.04		14.21	14.21	PC-DAG-33:2	0	0.04	1.9	15.16	35.3
DGCC-42:6	0.14	8.91		13.99	28.2	DGCC-27:0	0.04	0.02	1.45	0.78	37.62
PI-AR	0.05	4.14		6.5	34.71	PE-DAG-34:2	0.03	0	1.35	1.44	21.16
PC-DAG-33:2	0.04	3.71		5.83	40.54	PI-AR	0.06	0.05	1.3	1.6	20.86
MGDG-28:0	0.04	3.44		5.41	45.95	DGCC-26:0	0.04	0.01	1.26	0.89	20.2
PE-DAG-33:2	0.03	2.52		3.97	49.92	DGDG-34:2	0	0.03	1.25	1.17	2
PE-DAG-31:2	0.03	2.14		3.37	53.28	PE-DAG-31:2	0	0.03	1.21	4.58	19.3
Cluster 4: Average Similarity = 63.64						PE-DAG-33:1	0.03	0.01	1.2	1.46	19.73
IPLs	Average Cluster 2	Average Similarity	Similarity/S	Contribution (%)	Cumulative (%)	PE-DAG-33:3	0	0.02	1.16	4.61	51.59

308
309
310
311
312
313
314
315
316
317

318 **3.3 Distribution of alkyl chains based on length and degree of unsaturation**

319
320 The difference in the total number of acyl carbon atoms in both alkyl chains, rather than in individual fatty acids,
321 and in the number of acyl double bonds within each cluster is shown in Fig. 4. Statistical differences of IPLs
322 classes within each cluster was obtained through a Tukey HSD post-hoc test at a significant level of $p < 0.05$ (Fig.
323 4a, b). The average number of carbon atoms in the diglyceride moieties of IPLs in the Cluster 1 presented that
324 DGCC, MGDG, Others, PC, and PG were all distinct from one another ($n = 283$; $P < 0.05$; Fig. 4a). PG and Others
325 were characterized by relatively long alkyl chains (35-36 C atoms, respectively) and DGCC for shorter alkyl
326 chains (32 C atoms). In general, Cluster 1 exhibited a wide range of chain lengths among DAGs (28-36 C atoms).
327 Cluster 2 showed a narrower range than Cluster 1 (30-36 C atoms). This cluster also displayed no statistical
328 difference ($p > 0.05$) among IPL classes (Fig. 4a), following pairwise comparisons with Tukey's HSD post-hoc
329 test, despite the wide range of DGCC structures. Cluster 3, while it exhibited low variability in betaine lipids, it
330 also revealed the highest number of carbon atoms in DGCCs (42). On the contrary, Cluster 4 presented high
331 viability in DGCCs, which did not exceed 42 carbon atoms. Within the phospholipid class, PG showed the highest
332 number of carbon atoms in all clusters, the mean we observed was 34 carbon atoms and a range of 32-37 (Fig.
333 4a). The un-cluster sample (hadal sediment of 0-1 cm at A4 station) was characterized by relatively longer alkyl
334 chains (up to 42 C atoms) than Cluster 1 (Fig. 4a).

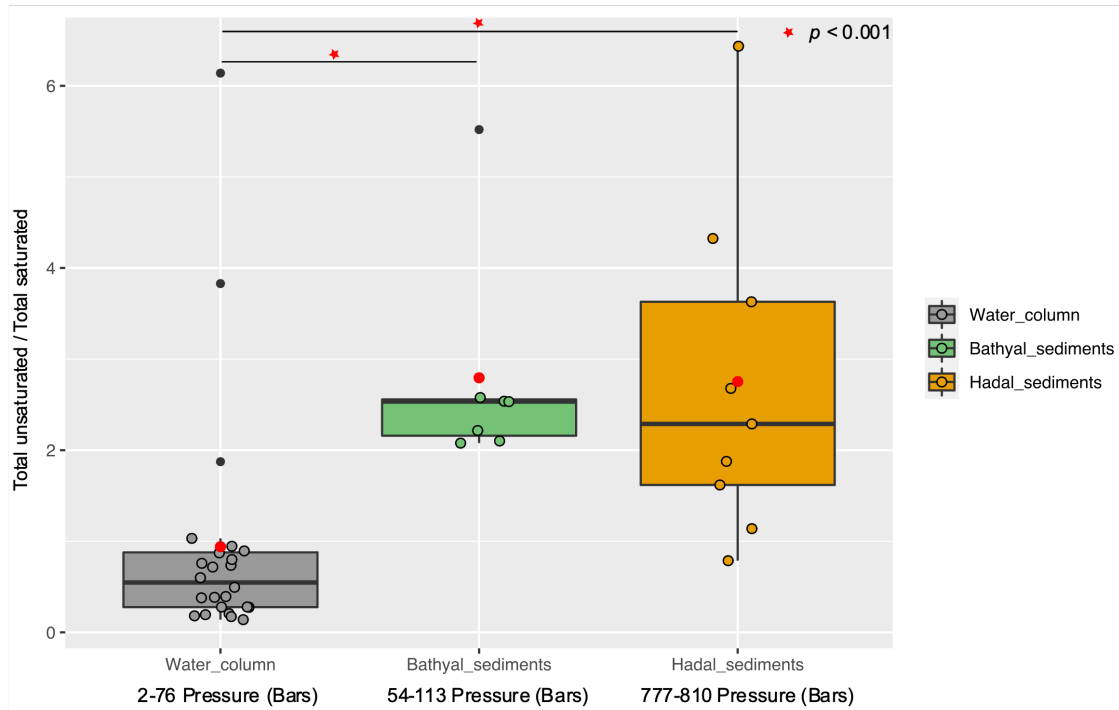
335
336 Overall, the degree of unsaturation (i.e., number of double bounds) within clusters was variable (Fig. 4b). Cluster
337 1 predominantly consisted of fully saturated and mono-unsaturated IPLs, except for PG that showed 2 double
338 bonds in average. In Cluster 2, the fatty acids of DGCCs were distinctly variable, although they exhibited 2
339 unsaturations on average. A similar pattern was observed in DGDGs with an average of 2.5 unsaturations (Fig.
340 4b). DGTS, MGDGD, PC and SQDG showed zero to 1 unsaturation, whereas DGTa, PE and PG exhibited
341 between 1 and 2.5 unsaturations. Cluster 3 showed more than 5 unsaturations on average for DGCC, unlike other
342 IPL classes that did not exceed 2 unsaturations. In Cluster 4, PG and DGCC presented ~3 and ~5 unsaturations
343 on average. Also, on average, DGDG and SQDG exhibited 2 unsaturations, MGDG and Others were mono-
344 unsaturated, and DGTS were saturated (Fig. 4b). Additionally, the ratio of total unsaturated fatty acids to total
345 saturated fatty acids in IPLs increased from (on average) ~0.9 in all water column samples (2-76 Bars) to ~2.7 in
346 the bathyal (54-113 Bars) and hadal sediments (777-810 Bars) (Fig. 5).



347
348
349
350
351

Figure 4. Total number of acyl carbon atoms (a) and acyl double bonds (b) in IPL classes across the distinct clusters shown in Fig. 2. The letters “a” and “b” indicate the presence of statistically distinct groups ($p < 0.05$) from both ANOVA and post-hoc Tukey HSD tests, respectively.

352
353



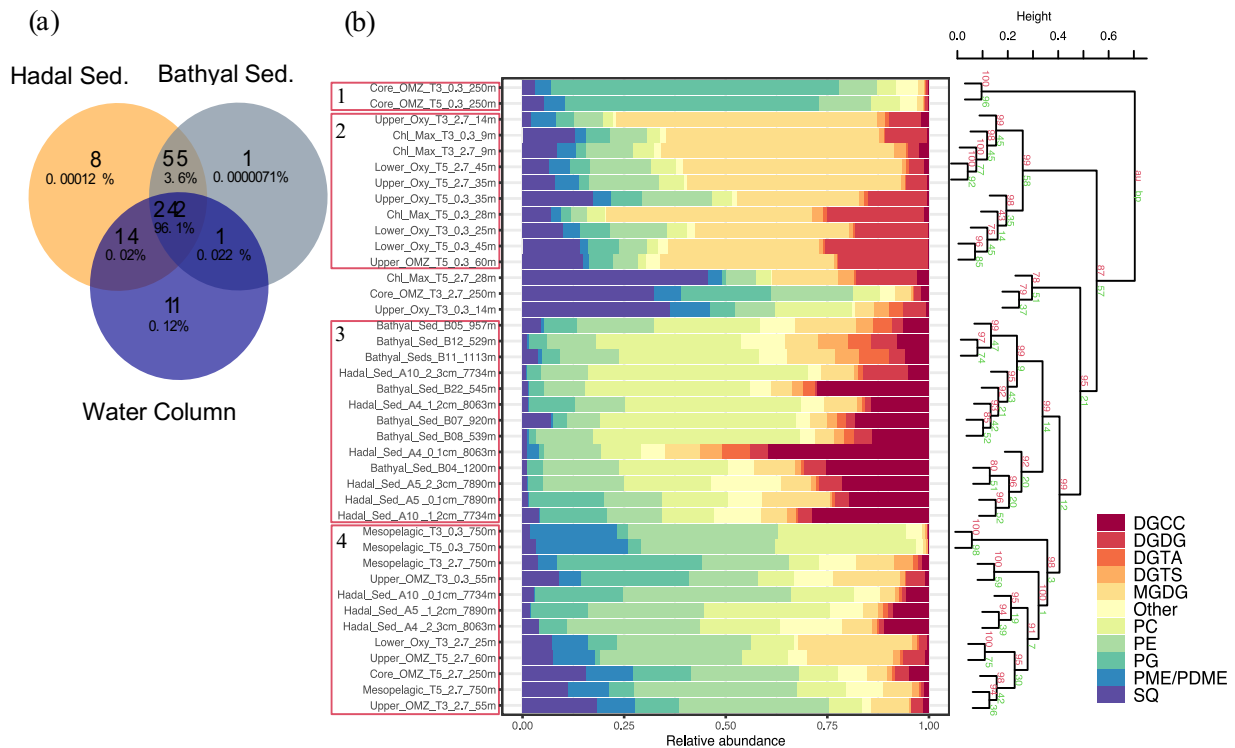
354
355
356
357
358
359
360

Figure 5. Boxplot showing the ratio of total unsaturated fatty acids to total saturated fatty acids derived from IPLs present in water column samples (Cantarero et al., 2020) and sediments of the Atacama Trench (this study). Red circles indicate the average value in each environment. Wilcoxon test (p -value < 0.001) indicates that sediments have statistical ratios higher than the water column (horizontal lines and red stars).

361 **3.4 Unique IPLs in hadal sediments of the Atacama Trench**

362
363 Water-column particles and bathyal-hadal sediments shared 242 (96.1%) IPL structures (Fig. 6a), while hadal
364 sediments and water-column particles shared 14 (0.02%), and hadal and bathyal sediments shared 55 (3.6%). Of
365 all the analyzed IPLs reported in this study, eight of them were unique to the Atacama Trench sediments and are
366 not present in shallower sediments nor the overlying water column. They include five glycolipids (SQDG-42:11,
367 SQDG-23:0, DGDG-35:1, DGDG-35:2 and DGDG-37:1), two phosphatidyl-inositol (PI-diOH-Ext-AR and PI-
368 OH-AR), and one ornithine lipid (OL-37:6). While unique to hadal sediments, their total concentration was low
369 (~53.32 ng g⁻¹ sediment) and they contributed ~0.00012% of the total IPL pool (Fig. 6a). We then performed a
370 cluster analysis to compare IPLs in deep-sea surface sediments against IPLs reported in the overlying water
371 column (Cantarero et al., 2020; Fig. 6b). Cluster 1 comprised samples from the core OMZ in the free-living
372 fraction (AU p-value of 100%). Cluster 2 comprised samples from both the upper and lower oxyclines (~14-60
373 m) as well as from the chlorophyll maximum (AU p-value of 99%). Cluster 3 comprised bathyal and hadal samples
374 (AU p-value of 99%). Cluster 4 mostly comprised the deepest water column sample (mesopelagic region at 750
375 m) and hadal samples (AU p-value of 98%; Fig. 6b). We also compared IPLs in hadal and bathyal sediments
376 against the pool of IPLs reported as diagnostic of the planktonic community inhabiting the chlorophyll maximum
377 in the upper water column (Cantarero et al., 2020), and thus assess their export and stability through their transit
378 to the deep-sea. Notably, these IPLs from this region of the water column only represent ~0.001-0.005% and
379 0.002-0.03% of the total IPL pool in hadal and bathyal sediments, respectively (Fig. S3).

380



381
 382 **Figure 6. Comparison of IPLs in bathyal and hadal sediments (this study) and the overlying water column (Cantarero
 383 et al., 2020).** (a) Venn diagram showing the number and percentage of unique and shared IPL molecules between these
 384 three environments. (b) Cumulative bar charts of IPL fractional abundances in each sample. Samples were grouped
 385 according to arithmetic mean (UPGMA) hierarchical clustering based on Euclidean distances. The cluster analysis on
 386 the right-hand size shows approximately unbiased (AU) and bootstrap probability (BP) in red and green numbers,
 387 respectively, whereas p-values are shown at branching points. Clusters with AU $\geq 95\%$ confidence are highlighted in
 388 red on the left-hand side.

391 We found a high degree of heterogeneity in total IPL concentrations among sites and different sediment levels (0–
 392 1, 1–2, 2–3 cm) in the Atacama Trench, which were an order of magnitude higher than bathyal sediments (see
 393 Figs. S4a, S4b). Hadal sediments at station A10 (7,734 m) showed a large range of phospholipid concentrations
 394 (~47–2,698 ng g⁻¹ sediment) (Fig. S4b). Although the highest total IPL abundances were observed at hadal station
 395 A10 (Fig. S4b), the greatest diversity in IPL composition was observed in the 0–1 cm of the hadal station A4,
 396 previously referred to as un-clustered (see Fig. 2). The most abundant IPL class in hadal sediments were
 397 phospholipids, PCs (~41–2,698 ng g⁻¹ sed.), PEs (~26–1,813 ng g⁻¹ sed.) and PGs (5–937 ng g⁻¹ sed.). The
 398 concentration of IPLs normalized by TOC (ng IPL/g TOC) showed maximum values in the hadal station A10
 399 (~497 µg IPL/g TOC), followed by lower values in the hadal stations A5 and A4 of ~291 and ~75 µg IPL/g TOC,
 400 respectively (Fig. S5).

4. Discussion

4.1 Potential sources of phospholipids

PG (Phosphatidylglycerol)

408 Phospholipids are common constituents of cellular membranes in most microorganisms (Ratledge and Wilkinson,
409 1988). Since PGs play an essential role in photosynthesis (Wada and Murata, 2007), they have therefore been
410 mainly identified in algal and bacterial photoautotrophs (Dowhan, 1997; Sato et al., 2000; Gombos et al., 2002).
411 However, their biological origin is highly diverse, and also includes heterotrophic bacteria (Oliver and Colwell,
412 1973; Van Mooy et al., 2009; Popendorf et al., 2011b; Carini et al., 2015; Sebastián et al., 2016), methylotrophs
413 (Batrakov and Nikitin, 1996), methanotrophic bacteria (Makula, 1978), *Pelagibacter ubique* (Van Mooy et al.,
414 2009), and barophilic bacteria (e.g., DB21MT-2 and DB21MT-5) isolated from sediments from the Marianas
415 Trench (Fang et al., 2000).

416
417 The hierarchical cluster analysis on variations in the relative abundance of PGs suggests that several compounds
418 maintained a similar proportion in bathyal and hadal sediments, which differs from the water column (Fig. S6).
419 Most PGs in the bathyal and hadal sediments have long acyl carbon chains (C₃₄-C₄₁), and they show odd- and
420 even-numbered polyunsaturated fatty acids (Fig. S6). The average chain-lengths of even-numbered *n*-C₁₈, *n*-C₂₀
421 and *n*-C₂₂ fatty acids, mostly in PCs and PGs, are indicative of algal inputs (Kaneda, 1991; Thompson Jr, 1996;
422 Bergé and Barnathan, 2005; Brandsma et al., 2012). However, since these PGs were not dominant in the water
423 column, a source from deeper environments is likely. Specifically, PG-DAG-36:2, PG-DAG-35:2, PG-DAG-36:5,
424 PG-DAG-37:2, and PG-DAG-41:4 are the dominant constituents of this IPL class in hadal-bathyal sediments (Fig
425 7; Fig. S6). PG-DAG-36:2 has been described in surface waters of the North Sea and also detected in
426 picoeukaryotes (Brandsma et al., 2012), and in heterotrophic bacteria in surface waters of the open South Pacific
427 Ocean (Van Mooy and Fredricks, 2010). However, these PGs are not dominant in the water column near the
428 Atacama Trench (Cantarero et al., 2020). On the other hand, PG-DAG-35:2, PG-DAG-36:5, PG-DAG-37:2 and
429 PG-DAG-41:4 are not commonly reported in water-column studies. Thus, it is possible that PGs present in the
430 Atacama Trench sediments derive from *in situ* microbial production, although downslope and lateral transport of
431 labile OM cannot be ruled out. PG-DAG-36:2 (Fig. 3) is the PG contributing most to the dissimilarity within the
432 cluster containing only hadal sediments (Cluster 1 in Figure 2). Thus, this lipid appears to be more representative
433 of *in situ* microbial production in this environment.

434
435 **PE (Phosphatidylethanolamine)**
436
437 PE and its methylated derivatives (PME, PDME) have been predominantly reported in membranes of diverse
438 bacterial sources, including heterotrophic bacteria (Van Mooy and Fredricks, 2010; Schubotz et al., 2018a),
439 nitrifying/denitrifying bacteria (Goldfine and Hagen, 1968), sulfate-reducing bacteria (Rütters et al., 2001; Sturt
440 et al., 2004), sulfur-oxidizing bacteria (Barridge and Shively, 1968; Imhoff, 1995; Wakeham et al., 2012),
441 methanotrophic bacteria (Makula, 1978; Sturt et al., 2004), and barophilic bacteria (Fang et al., 2000).

442
443 PEs showed a similar distribution in bathyal and hadal sediments (Fig. S7), where they are dominated by long-
444 chain (C₃₆₋₄₄) polyunsaturated fatty acids, contrary to the shorter chains (C₂₈₋₃₆) of saturated and monounsaturated
445 fatty acids present in the water column. PE-DAG-32:1, PE-DAG-32:2, and PE-DAG-33:1 are the dominant PE
446 compounds of bathyal and hadal sediments (Fig. 7). These IPLs have been previously reported in heterotrophic
447 bacteria (Van Mooy and Fredricks, 2010; Brandsma et al., 2012). On the other hand, fatty acids in PEs including
448 monounsaturated and polyunsaturated (e.g., C_{20:5} and C_{22:6}) have been reported in barophilic bacteria isolated from

449 sediments from the Marianas Trench (Fang et al., 2000). Thus, although we cannot confidently rule out other
450 sources, it is possible that PEs present in the AT sediments predominantly derive from *in situ* production by
451 barophilic heterotrophic bacteria. PE-DAG-32:1, PE-DAG-32:2 and PE-DAG-33:1 (Fig. 3) are the PEs that
452 contributed most to the dissimilarity within the cluster containing only hadal sediment samples (Cluster 1 in Figure
453 2). Thus, this cluster appears to be representative of *in situ* microbial production in this environment.
454

455 **PC (Phosphatidylcholine)**

456

457 PCs were amongst the most diverse (43 structures: Fig. S8) and abundant phospholipid class in hadal sediments
458 (Fig. S4). PC is the major membrane-forming phospholipid in eukaryotes (Lechevalier, 1988; Sohlenkamp et al.,
459 2003; Van Mooy et al., 2006; Van Mooy and Fredricks, 2010). Additionally, PC has been reported to be a major
460 DAG in zooplankton, from protozoa to copepods and krill (Patton et al., 1972; Mayzaud et al., 1999; Lund and
461 Chu, 2002). However, genomic data indicates that more than 10% of all bacteria possess the genetic machinery
462 for PC biosynthesis (Sohlenkamp et al., 2003). PC has also been reported in nitrifying bacteria (Lam et al., 2007),
463 photoheterotrophic bacteria (Kobližek et al., 2006; Van Mooy et al., 2006), and barophilic bacteria (Fang et al.,
464 2000). In surface sediments of the Black Sea (2000 m), PCs were related to algal material rapidly exported from
465 surface waters (Schubotz et al., 2009a).
466

467

468 Hadal and bathyal sediments, in addition to two OMZ core stations, were clustered in the PC class (AU p-value
469 of 97%; Fig. S8). This cluster showed PCs with long (C₃₃₋₃₈) and polyunsaturated fatty acids (up to 10
470 unsaturations). The dominant constituents were PC-DAG-35:0, PC-DAG-30:2, PC-DAG-30:1, PC-DAG-33:2,
471 PC-DAG-35:1, PC-DAG-29:2, PC-DAG-32:1, and PC-DAG-36:2 (Fig. 7; Fig. S8). PC-DAG-36:2 and PC-DAG-
472 30:1 have been associated with phytoplankton detritus (Schubotz et al., 2009a) and bacteria (Brandsma et al.,
473 2012), whereas PC-DAG-32:1 has been associated with picoeukaryotes (Brandsma et al., 2012).
474

475

476 Since the most abundant PCs in Cluster 1 have not been reported as dominant structures in any specific
477 environment before, they are possibly produced *in situ*, although downslope and/or lateral transport cannot be
478 ruled out. Among bacteria, those membranes reported to contain PC belong to the alpha and gamma subgroups of
479 the proteobacteria (Sohlenkamp et al., 2003). Given that these bacterial groups are abundant in trench samples
480 from Puerto Rico (Eloe et al., 2011), the Mariana (Nunoura et al., 2015) and recently in the Atacama Trench
481 (Schauberger et al., 2021), it is possible that PCs present in high abundance in the Atacama Trench are consistent
482 with high abundance of proteobacteria in these regions. Given their general known association and abundance in
483 Atacama Trench sediments (Fig. S4), they likely derive primarily from bacterial, but also possibly from fungi or
484 metazoan sources that have not yet been studied, and to a lesser extent from phytoplankton. Indeed, fungal strains
485 isolated from the water column and sediment in the ESTP off Chile reported high levels of polyunsaturated fatty
486 acids and PCs (Gutiérrez et al., 2020), whereas a high fungal diversity associated with denitrification potential
487 was reported in the Yap Trench (Gao et al., 2020). The latter suggests that eukaryotic PCs in hadal sediments
488 could be much more diverse in origin than previously thought.
489

488 **PME/PDME (Phosphatidyl(di)methylethanolamine)**

489

490 PME/PDMEs have been observed in association with methanotrophic bacteria (Makula, 1978; Goldfine, 1984;
491 Fang et al., 2000), sulfide oxidizer bacteria (Barridge and Shively, 1968), sulfate-reducing bacteria, mainly
492 *Desulfobulbus spp* (Rossel et al., 2011), Proteobacteria (Oliver and Colwell, 1973; Goldfine, 1984), and barophilic
493 bacteria from the Mariana Trench (Fang et al., 2000). Additionally, the occurrence of PME-DEG at some hadal
494 stations suggests the presence of sulfate-reducing bacteria (Rütters et al., 2001; Sturt et al., 2004).

495 PME/PDMEs exhibited their lowest abundance ($\sim 10 \text{ ng g}^{-1} \text{ sed}^{-1}$) in sediment samples compared to other
496 phospholipids (Fig. S4b). In the bathyal and hadal sediments they were clustered (AU p-value of 97%) and
497 dominated by PDME-DAG-33:1, PME-DAG-37:2, PME-DAG-34:2, PME-DAG-31:1, and PME-DEG-33:0 (Fig.
498 S9a). PME-DEG-33:0 has been shown to correlate with high NO_2^- in the overlying water column of this area
499 (Cantarero et al., 2020), which could suggest a potential association with denitrification processes. These
500 structures have also been reported in the deep chemocline of the Cariaco basin (Wakeham et al., 2012), suggesting
501 a potential chemoautotrophic and/or heterotrophic source. The distribution of these compounds is different from
502 the water column, which is dominated by the saturated PME-32:0, PME-DAG-30:0, and PME-DAG-31:0 (Fig.
503 S9a and S16; Cantarero et al., 2020). Thus, and similar to other lipid classes, they most likely derive from *in situ*
504 production in hadal sediments rather than from the water column, although other sources such as downslope and/or
505 lateral transport cannot be ruled out. No particular PME/PDME were found to contribute to the dissimilarity
506 between the cluster containing only hadal sediment samples (Cluster 1 in Figure 2) and other sediment samples.
507

508 **4.2 Potential sources of glycolipids**

509

510 **MGDG (Monoglycosyldiacylglycerol)**

511

512 Due to their dominant occurrence in chloroplast thylakoid membranes (Murata and Siegenthaler, 1998) and
513 particularly in cyanobacteria (Heinz, 1977; Harwood, 1998; Wada and Murata, 2007; Van Mooy and Fredricks,
514 2010), but also in heterotrophic bacteria (Popendorf et al., 2011b), MGDGs are probably the most abundant IPLs
515 on earth (Gounaris and Barber, 1983).

516 The hierarchical cluster groups MGDGs in bathyal (AU p-value of 90%) and hadal (AU p-value of 98%)
517 sediments (Fig. S10). The most abundant MGDGs in the bathyal and hadal sediments were MGDG-28:0, MGDG-
518 32:1, MGDG-30:1, MGDG-32:0 and MGDG-37:3. MGDG-28:0, and MGDG-30:1, which are ubiquitous along
519 the oxycline of the overlying OMZ (Fig. 7; Cantarero et al., 2020), in addition to MGDG-32:1. MGDG-32:0 has
520 been reported in waters of the eastern south Pacific (Van Mooy and Fredricks, 2010). Thus, the occurrence of
521 these MGDGs in sediment could indicate at least some export of labile OM from surface waters. On the other
522 hand, MGDG-37:3 does not appear to be a dominant structure in any specific environment in the literature, which
523 suggests a likely *in situ* production.

524

525 **DGDG (Diglycosyldiacylglycerol)**

526

527 DGDGs are commonly found in membranes of eukaryotic algae and cyanobacteria (Wada and Murata, 1998;
528 Sakurai et al., 2006; Kalisch et al., 2016). DGDGs clustered together in bathyal and hadal sediments (AU p value
529 of 96%) whereas their distribution differed from the water column (Fig. S11). The most abundant DGDGs in hadal
530 and bathyal sediments of the Atacama Trench was DGDG-34:2 (Fig 7), which has been previously reported in

531 cyanobacterial strains isolated (da Costa et al., 2020), but has not been previously reported as abundant in the
532 water column. In contrast, DGDG-30:0, which is widely distributed in the water column of this region (Cantarero
533 et al., 2020), is consistently present in hadal and bathyal sediment samples although at very low abundances (Fig.
534 7). Thus, although DGDGs account for less than ~5% of the total IPL pool (Fig. 6b), except for station A10 (2-3
535 cm) where they reach ~10%, their presence in bathyal and hadal sediments is indicative of at least some export of
536 labile OM from surface waters.

537

538 **SQDG (Sulfoquinovosyldiacylglycerol)**

539

540 SQDG are predominantly produced by photoautotrophs (Van Mooy et al., 2006; Popendorf et al., 2011b),
541 including various groups of diatoms, brown and green algal chloroplast membranes (Harwood, 1998), and
542 cyanobacteria (Siegenthaler, 1998; Wada and Murata, 1998). SQDGs have also been found in bacteria from the
543 α - and γ -proteobacterial lineages (Benning, 1998). In the overlying water column of the Atacama Trench,
544 Cantarero et al., (2020) suggested a higher contribution of SQDGs from cyanobacteria than algae. Also, SQDGs
545 found in the deep Atlantic (down to ~4,000-5,000 m) appear to indicate a source and export from surface waters
546 (Gašparović et al., 2018).

547

548 SQDGs showed a consistent distribution in bathyal and hadal sediments, where they are dominated by long-chain
549 (C_{36-44}) fatty acids (Fig. S12). This is contrasting to their distribution in the overlying water column where they
550 are dominated by shorter chain (C_{28-36}) saturated fatty acids (Cantarero et al., 2020). SQDG-30:0, SQDG-32:0,
551 SQDG-30:2, and SQDG-38:4 were the dominant SQDG constituents of bathyal and hadal sediments (Fig. 7).
552 SQDG-30:0 and SQDG-30:2 have been reported in bacteria in North Sea surface waters (Brandsma et al., 2012),
553 in cyanobacteria of the eastern subtropical South Pacific (Van Mooy and Fredricks, 2010), and in plankton detritus
554 from surface sediments of the Black Sea (Schubotz et al., 2009a). Furthermore, SQDG-30:0 is abundant in surface
555 waters of our study area and SQDG-38:4 has been correlated with NO_3^- (Cantarero et al., 2020). The observed
556 differences in the distribution of SQDGs in deep sediments compared to the water column suggests an *in situ*
557 production of previously poorly characterized compounds, in addition to at least some export from surface waters.

558

559 **4.3 Potential biological sources of betaine lipids**

560

561 **DGTS (Diacylglyceryl trimethylhomoserine)**

562

563 DGTSs have diverse biological origins, being found in a wide range of eukaryotes (Sato, 1992; Dembitsky, 1996;
564 Kato et al., 1997; Van Mooy et al., 2009), photoheterotrophic bacteria (Benning et al., 1995; Geiger et al., 1999),
565 photoautotrophic bacteria (Popendorf et al., 2011b) including cyanobacteria (Řezanka et al., 2003), and members
566 of the α -Proteobacteria subdivision (López-Lara et al., 2003). Schubotz et al. (2018) showed DGTS with varying
567 fatty-acid compositions in the OMZ system of the eastern tropical North Pacific, especially in OMZ waters,
568 indicating that these compounds can be biosynthesized by a wider range of source organisms than previously
569 thought.

570 Consistent with other IPL classes, DGTSs of the bathyal and hadal samples were grouped in the same cluster (AU
571 p-value of 98%) and differed from the water column (Fig. S13). However, several DGTSs are shared between

572 surface waters (9-60 m) and deep sediments. Indeed, the most abundant DGTSS in bathyal and hadal sediments
573 (DGTS-34:0, DGTS-32:1, DGTS-26:0, DGTS-34:1, DGTS-32:0, and DGTS-25:0; Fig. 7; Fig. S13) are also
574 prominent in the chlorophyll maximum in the eastern subtropical South Pacific (Van Mooy and Fredricks, 2010,
575 and Cantarero et al., 2020). Therefore, their presence in hadal sediments suggest the export of some labile OM
576 from the euphotic zone, although we cannot rule out other sources.

577

578 **DGTA (Diacylglycerol hydroxymethyl- β -alanine)**

579

580 DGTAs have been widely reported in eukaryotic phytoplankton (Araki et al., 1991; Dembitsky, 1996; Cañavate
581 et al., 2017), mainly in diatoms (Volkman et al., 1989; Zhukova, 2005; Gómez-Consarnau et al., 2007), and are
582 also especially abundant in cultures of Prymnesiophytes and Cryptophytes (Kato et al., 1997). DGTAs have also
583 been found in cyanobacteria (Brandsma et al., 2012) and heterotrophic bacteria (Popendorf et al., 2011a; Sebastián
584 et al., 2016).

585 DGTAs in bathyal and hadal sediments are mainly composed of longer (C₂₈-C₄₂) and polyunsaturated (1-12) fatty
586 acids compared to those present in the shallowest region of the overlying water column, composed of shorter and
587 saturated fatty acids (Fig. S14). In the overlying water column, these compounds are associated with relatively
588 high chlorophyll and O₂ concentrations (Cantarero et al., 2020), similar to North Sea surface waters (Brandsma et
589 al., 2012). To the best of our knowledge, the dominant DGTAs in hadal and bathyal sediments (Fig. 7; Fig. S14)
590 have not been previously reported as dominant IPLs in other environments. Whereas no specific biological sources
591 in hadal sediments are known, the structures containing between 30 and 38 carbon atoms might be characteristic
592 of this type of environment.

593

594 **DGCC (Diacylglycerolcarboxy-N-hydroxymethyl-choline)**

595

596 Our knowledge of DGCC sources is limited. They have been found in membranes of Prymnesiophyte algae (Kato
597 et al., 1994), mainly in *Pavlova lutheria* (Kato et al., 1994; Eichenberger and Gribi, 1997), and in *E. huxleyi*
598 (Volkman et al., 1989; Pond and Harris, 1996; Van Mooy and Fredricks, 2010). Additionally, they have also been
599 reported in the diatom *Thalassiosira pseudonana* (Van Mooy et al., 2009).

600 The most abundant IPL from the entire data set of Bathyal and hadal sediments is DGCC-42:6 (Fig. 7; Fig. S15).
601 This is the compound with the largest number of C atoms (42) and unsaturation (6) in all IPLs detected in this
602 study. DGCCs with long-chain, polyunsaturated fatty acids (i.e., C_{38:6}, C_{40:10}, C_{42:11}, C_{44:12}) have been previously
603 reported in phytoplankton (Hunter, 2015; Van Mooy and Fredricks, 2010). However, the most abundant DGCCs
604 in hadal sediments have, to the best of our knowledge, not been previously reported, which highlights their
605 potential as biomarkers of deep-sea sediments. However, 3 hadal stations clustered in a separate group (see Fig.
606 S15), were dominated by DGCC-27:0, and did not contain DGCC-42:6, indicating that this IPL probably derives
607 from allochthonous sources.

608

609

610

611

612

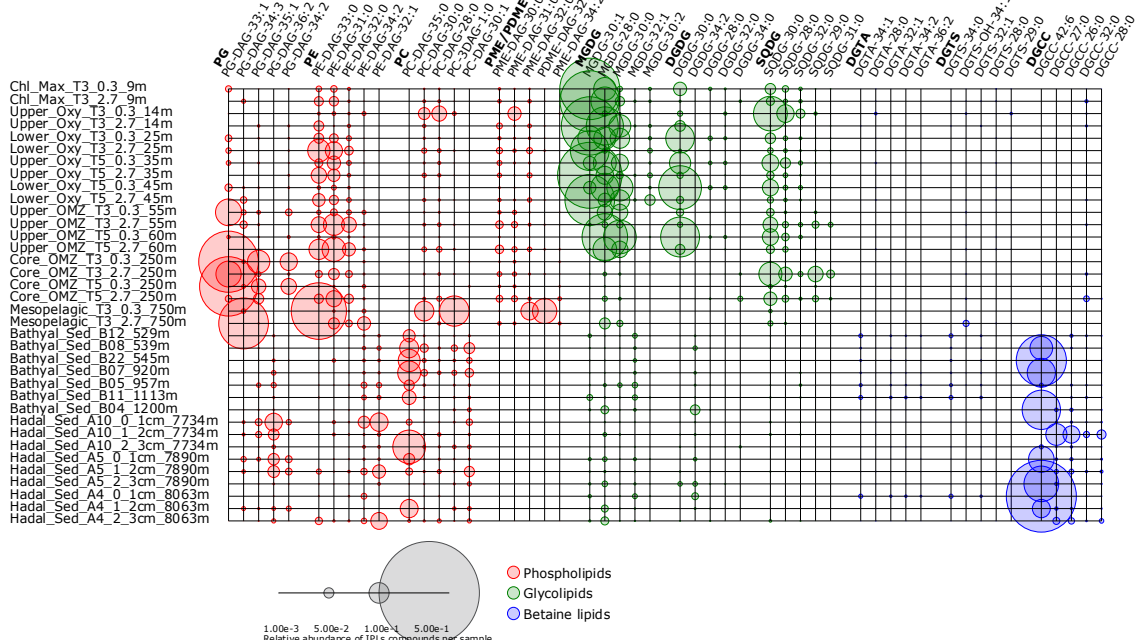


Figure 7. Relative abundance of the five most abundant individual IPLs contributing to each IPL class. Circle size is proportional to the relative abundance of IPL compounds per sample. Samples are organized along the Y axis by depth, whereas phospholipids, glycolipids, and betaine lipids are shown in colors. The legend provides a scale for circumference size.

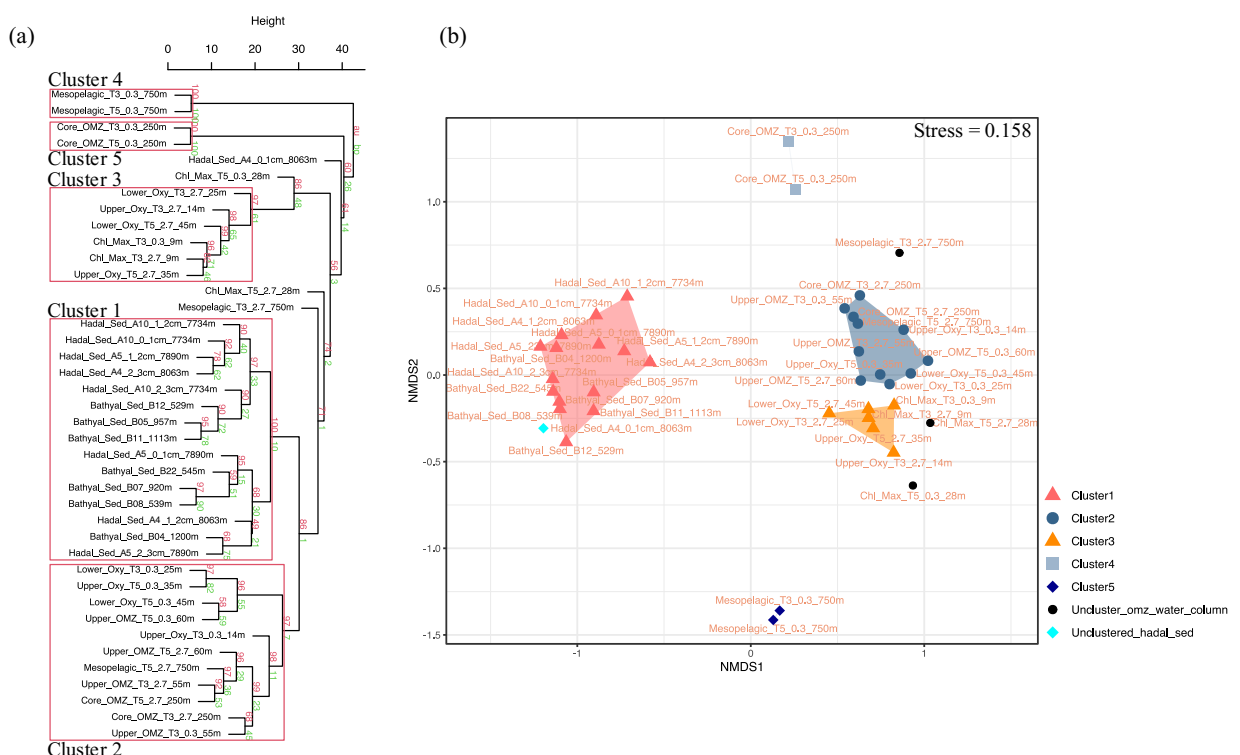
4.4 Potential biological sources of other lipids

Glycosidic ceramides (Gly-Cer) have been reported in eukaryotic algae such as Prymnesiophyte (Vardi et al., 2009), and have also been shown to be abundant in water columns of OMZ systems (Schubotz et al., 2009b, 2018; Cantarero et al., 2020). In general, the overlying water column shows Gly-Cer with ceramide chain, and polyunsaturated fatty acids with C₂₁₋₃₈. However, these structures are scarce in the bathyal and hadal sediments (see Fig. S9b), which could reflect a deficient export from surface waters due to intense remineralization. On the other hand, Ornithine lipids (OL), phosphatidylinositol (PI), PC-AEGs and other unidentified phospholipids were also present in deep sediments (Fig. S9b). Some PIs and OLs have been reported in sulfate-reducing bacteria (Sturt et al., 2004; Bühring et al., 2014), whereas PC-AEGs have been reported in bacteria inhabiting water columns with reduced oxygen concentration (Schubotz et al., 2018b). Thus, the high relative abundance of PC-AEG-34:3 in hadal and bathyal sediments (Figs. S9b and S16) could be indicative of anaerobic microbial processes. PC-AEG-34:3 contributed the most to the dissimilarity between the cluster containing only hadal sediment samples (Cluster 1 in Figs. 2, and 3), thus suggesting an *in situ* microbial production, although we cannot confidentially rule out other sources.

4.5 Allochthonous versus autochthonous IPLs in the Atacama Trench

Given their rapid degradation after cell death (White et al., 1979; Harvey et al., 1986; Logemann et al., 2011), IPLs are typically considered markers of living or recently dead cells (White et al., 1979; Harvey et al., 1986; Petersen et al., 1991; Lipp et al., 2008). The distribution of IPLs in bathyal and hadal sediments exhibits a high degree of similitude, as demonstrated by the hierarchical analysis (Cluster 1 in Fig. 8a), the NMDS (Fig. 8b), and the SIMPER analysis (Cluster 1 in Table S1). The deep-sea surface sediments showed weak clustering with the

IPLs reported in the overlying water column by Cantarero et al. (2020) (Fig 9a). Additionally, water column samples exhibit a larger degree of separation than sediments (ANOSIM, $R = 0.78$; $P < 0.01$; Fig. 8b) and are broadly clustered by geochemical environments (Cantarero et al., 2020). The low abundance of IPLs characteristic of organisms inhabiting the chlorophyll maximum in deep-sea sediments of the Atacama Trench ($<0.005\%$ of the total IPL pool; Fig. S3) suggests minimal export of labile organic compounds from the upper ocean. This result implies rapid IPL degradation during sinking in the water column, which is consistent with experimental degradation rates (Westrich and Berner, 1984; Logemann et al., 2011) and first-order POM sinking rates. Indeed, by using the experimentally calculated kinetic degradation rate constants (k') of ester-bound IPLs by Logemann et al. (2011), and the sinking rate of particles from surface waters to 4000 m (20-100 m/day; Billett et al., 1983; Danovaro et al., 2014), we calculated that $\sim 86\text{-}98\%$ ($k'_{t=80} = 0.033$ and $k'_{t=400} = 0.011$) of IPLs from surface waters should degrade by the time that particles reach depths of ~ 8000 m. These results are also in accord with studies indicating elevated benthic oxygen consumption rates resulting from intense microbial respiration of sinking OM reaching the sediment (Glud et al., 2013; Wenzhöfer et al., 2016). Thus, the pool of IPLs in hadal sediments appears to predominantly represent *in situ* microbial production, whereas the deep-sea microbial community in both bathyal and hadal sediments is similar despite their bathymetric zonation ($\sim 1,000\text{-}8,000$ m). Alternatively, we cannot rule out the possibility of new IPL production, particularly from heterotrophic and chemoautotrophic bacteria in micro niches of sinking particles reaching the deep-sea, and/or downslope and lateral sediment transport.



661 Cluster 2
 662 Figure 8. (a) Arithmetic mean (UPGMA) hierarchical clustering based on Euclidean distances calculated from IPLs in
 663 each sampling station. Red values are Approximately Unbiased (AU) p-values and green values are Bootstrap
 664 Probability (BP) for each node. Red boxes highlight clusters with 95% confidence. The number of bootstrap replicates
 665 is 10000. (b) Non-metric multidimensional scaling (NMDS) analysis of IPLs at each sampling station. The distance
 666 matrix was calculated based on the Bray–Curtis dissimilarity. The stress value of the final configuration was 15.8 %.
 667 Different symbols and colors represent the sample grouping from hierarchical clusters shown in panel a.
 668 Marine trenches receive organic carbon from a variety of sources and transport mechanisms. These include
 669 canyons and river systems that channel OM from land to coastal regions, aeolian transport, surface water

670 productivity, and *in situ* production, to name a few (Wenzhöfer et al., 2016; Tarn et al., 2016; Luo et al., 2017;
671 Xu et al., 2018; Guan et al., 2019; Xu et al., 2021). Carbon flux events can increase the delivery of particulate
672 carbon from surface waters to the seafloor (Poff et al., 2021), whereas river discharge and aeolian transport can
673 result in enhanced terrestrial carbon (Xu et al., 2021). Mass wasting events are also known to create dynamic
674 depositional conditions and strong spatial heterogeneity in OM distribution in marine trenches (Schauberger et
675 al., 2021; Xu et al., 2021). While marine organic carbon appears to dominate sediments in the Japan
676 (Schwestermann et al., 2021) Massau, and New Britain (Xu et al., 2020) trenches, the Atacama and Kermadec
677 Trenches, on the other hand, have been reported to be dominated by terrigenous OM. Since our study only focuses
678 on the most labile component of the total lipid pool, it predominantly traces labile and indigenous OM and not
679 recalcitrant fractions of the lipid pool. The latter warrants further investigation.

680

681 In regions like the Japan trench, downslope sediment transport has been linked to earthquake-driven
682 remobilization (Bao et al., 2018; Schwestermann et al., 2021). Whereas we lack sedimentological/geochemical
683 data to discriminate if the top 3 cm of our hadal stations represent debris flows, turbidite, or mass wasting events,
684 ongoing work in the Atacama Trench indicates heterogenic sediment deposition along the hadal zone (Matthias
685 Zabel., pers. communication). Thus, the role of downslope transport as a mechanism to explain the high statistical
686 similarity between bathyal and hadal sediments remains to be tested.

687

688 **4.6 Characteristic IPLs of hadal and bathyal sediments**

689

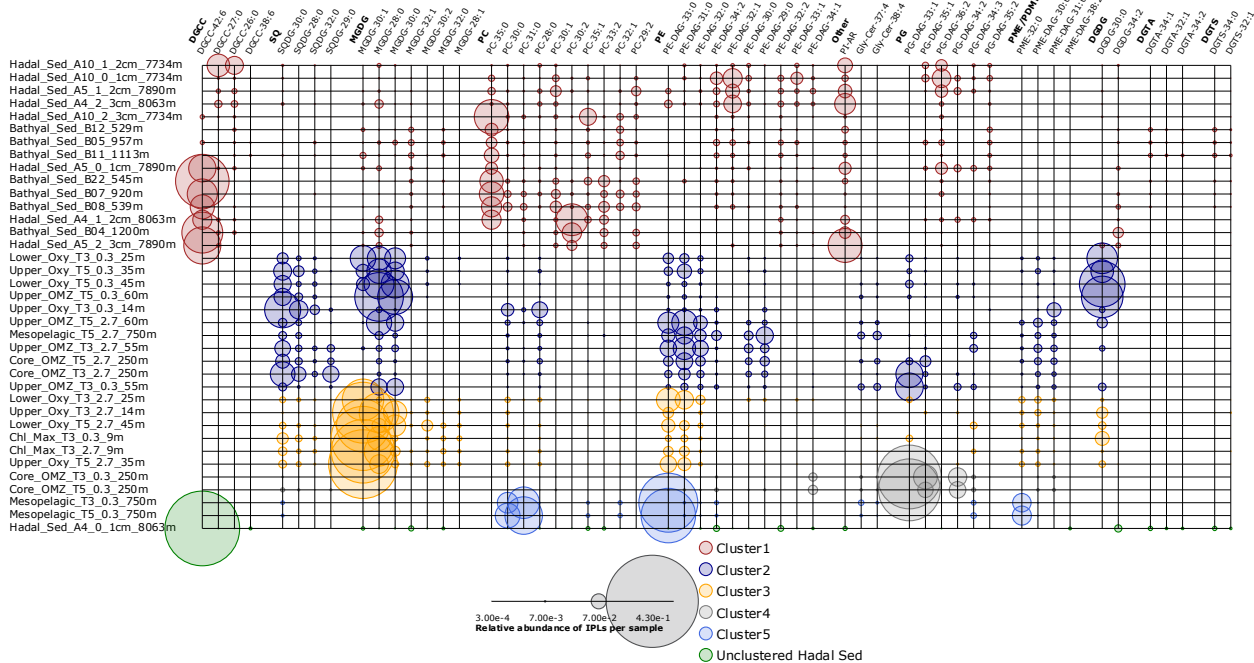
690 The IPLs that contribute most to the dissimilarity between the hierarchical cluster containing samples from the
691 hadal and bathyal sediments (Cluster 1 of Fig. 8) and the water column (cluster 2, 3, 4 and 5 of Fig. 8) are
692 represented in Fig. 9. The most characteristic IPLs of hadal and bathyal sediments are: DGCC-42:6, DGCC-27:0,
693 DGCC-26:0, PC-DAG-35:0, PC-DAG-30:1, PC-DAG-30:2, PC-DAG-33:2, PC-DAG-32:1, PC-DAG-29:2, PE-
694 DAG-32:1, PE-DAG-32:2, PE-DAG-33:1, PG-DAG-36:2, and DGDG-34:2, which we propose as potential
695 markers for these environments. Even though DGCCs have been mainly related to algae membranes (Kato et al.,
696 1994; Van Mooy et al., 2009), they are minor components of the water column in this area, suggesting the
697 occurrence of an alternative source. In addition to DGCCs, the two other betaine lipids, DGTA and DGTS,
698 exhibited five IPLs that were almost exclusively present in sediment samples (DGTA-34:1, DGTA-32:1, DGTA-
699 34:2, DGTS-34:0 and DGTS-32:1, see Figure 11). We note that almost all the PC phospholipids in our study have
700 not, to the best of our knowledge, been previously reported in the literature, which reinforces their use as markers
701 of sedimentary *in situ* bathyal and hadal production.

702

703 The presence of a few MGDGs and SQDGs in hadal and bathyal sediments (~7% of the total IPL pool) indicates
704 that at least some labile OM could derive from the shallow water column (see section 4.2). However, the most
705 abundant IPLs in our sediment samples, DGCC-42:6, PC-DAG-35:0, PE-DAG-32:1 and PG-DAG-36:2 (19.8%
706 of the total IPL pool; Fig. S16), are almost completely absent in the overlying water column (Fig. 9). This
707 reinforces the idea that these IPLs most likely originate from *in situ* microbial production in sediments. The single
708 most abundant IPL in sediments, DGCC-42:6, was not present in cluster 1, which only contains hadal sediments
709 (Figs. 2 and 3). Instead, this compound is prominent in clusters 3, 4, and 5, containing both hadal and bathyal

710 samples. Thus, DGCC-42:6, as well as PC-DAG-35:0, which has the lowest relative abundance in the cluster with
711 only hadal sediments, could be indicators of downslope transport from bathyal to hadal regions.

712 We acknowledge that temporal variability in IPL production in the water column and sediment, as well as the lack
713 of data on the largely uncharacterized hadal endemic microbial community, could complicate some of the
714 phylogenetic and source associations of IPLs and warrant further investigation. Despite this, our study represents
715 a step forward on the characterization of labile sources of OM sustaining hadal ecosystems.



718
 719 **Figure 9.** Relative abundance of individual IPLs that contribute most to the dissimilarity between clusters of Fig. 8
 720 derived from the SIMPER analysis (Table S1). Circle size is proportional to the relative abundance of IPL compounds
 721 per sample. Samples are organized along the Y axis and shown in colors that match the hierarchical cluster analysis in
 722 Fig. 8. The legend shows the scale for circumference size.

725 4.7 Do IPLs reveal homeoviscous adaptation to the deep-sea environment?

Environmental factors such as pH, conductivity, temperature, and pressure impact the permeability and fluidity of cell membranes (Shaw, 1974; Macdonald, 1984; DeLong and Yayanos, 1985; Somero, 1992; Komatsu and Chong, 1998; Van Mooy et al., 2009; Carini et al., 2015; Sebastián et al., 2016; Siliakus et al., 2017; Boyer et al., 2020). Thus, organisms adapt to changes in environmental factors to maintain physiological homeostasis by altering their fatty acid composition (DeLong and Yayanos, 1985; Fang et al., 2000; Nichols et al., 2004; Siliakus et al., 2017). For instance, the combined physiological effects of high hydrostatic pressure and low temperature on prokaryotic membranes in laboratory cultures leads to the production of unsaturated lipids (DeLong and Yayanos 1985; Fang et al., 2000; Nichols et al., 2004; Zheng et al., 2020). However, few studies have been conducted using culture-independent techniques in search for potential adaptation mechanisms in organisms inhabiting the deep ocean (i.e., Zhong et al., 2020). We sought to understand whether the chemical composition of core fatty acids within different IPL classes (i.e., carbon length and unsaturation degree) reflects the combined

738 effects of the low temperature and high pressure typical of hadal settings. We show that PGs are abundant in hadal
739 sediments of the Atacama Trench (Fig. S4). Bacterial strains isolated from Mariana Trench sediments contain PG
740 as the most abundant class of phospholipids (Fang et al., 2000), which these authors presumed it could represent
741 a physiological response to high pressure and low temperature. This has been confirmed by subsequent studies
742 (Winter et al., 2009; Periasamy et al., 2009; Jebbar et al., 2015, Allemand et al., 2021). Cluster 1 in the boxplot
743 analysis (Fig. 4) likely contains the most characteristic IPL classes of the hadal zone. In general, the phospholipids
744 in this cluster exhibited fatty acid chains that are monounsaturated and saturated compared to other environments
745 (Figs. 4a, b). Additionally, we observed an increase in the ratio of total unsaturated to saturated fatty acids in deep
746 sediments compared to the water column (Fig. 5), which could reflect physiological adaptations of their biological
747 producers. These results are in accord with studies indicating biosynthesis and incorporation of polyunsaturated
748 fatty acids into phospholipid membranes of piezophilic bacteria (DeLong and Yayanos, 1985; Baird et al., 1985;
749 Yano et al., 1998; Winter, 2002; Mangelsdorf et al., 2005; Winter and Jeworrek, 2009; Allemand et al., 2021).
750 Thus, the chemical characteristics (C length and degree of unsaturation) of the most abundant IPLs in sediments
751 of the Atacama Trench suggest homeoviscous adaptation to this type of environment by their source organisms,
752 in addition to potentially indicating the occurrence of compounds that are unique to the endogenous community.
753

754 **5. Conclusions**

755

756 Bacterial and eukaryotic IPLs in surface hadal sediments from the deepest points of the Atacama Trench share
757 characteristics with those in bathyal sediments and differ from those found in suspended particles from the upper
758 750 m of the water column, including the oxygen minimum zone. This indicates that: a) most IPLs abounding the
759 upper water column are almost entirely degraded during their descent to the hadal seafloor, and b) IPLs found in
760 hadal sediments are predominantly derived from in situ microbial communities.

761

762 The most dominant ester-bound IPL structures found in bathyal and hadal sediments show a great variety of
763 phospholipids with varying degrees of unsaturation, most of them yet to be described, that are likely derived from
764 yet poorly characterized bacterial and/or eukaryotes sources. Hadal sediments also exhibit unique glycolipid
765 structures, such as SQDG-42:11, SQDG-23:0, DGDG-35:1, DGDG-35:2 and DGDG-37:1, that to the best of our
766 knowledge, have not been reported in other environments. However, these lipids are present in low abundance
767 and represent a small fraction (~0.00012%) of the total IPL pool. Furthermore, elevated ratios of
768 unsaturated/saturated fatty acids in hadal sediments are likely indicative of homeoviscous adaptation to the high
769 pressure and low temperatures characteristic of this extreme deep-sea environment.

770

771 An improved understanding of the phylogenetic, ecological, and metabolic association of IPLs present in the
772 Atacama Trench could be achieved in future studies by the pairing of lipidomics with genomic techniques (e.g.,
773 microbial community composition, functional groups, lipid biosynthesis), in addition to a detailed
774 sedimentological and biogeochemical characterization of sediments.

775

776 **Author contribution**

777

778 EF, OU, and JS designed the study. MZ contributed with the hadal samples from the HADES-ERC cruise. EF
779 prepared, extracted, and analyzed samples from the HADES-ERC cruise with help from SC and ND under the
780 supervision of JS. EF and SC processed results. EF, SC, and JS interpreted results. EF and PR-F performed
781 statistical analyses. EF wrote the manuscript with contributions from SC, JS, and OU. All authors provided
782 feedback on the manuscript. OU and JS funded the research.

783

784

785 **Competing interests**

786

787 The authors declare that they have no conflict of interest.

788

789 **Acknowledgements**

790

791 This work was supported by the Chilean Agency for Research and Development (grants ICN12_019-IMO and
792 FONDECYT 1191360 to O. Ulloa). Additional support was provided by the Department of Geological Sciences
793 and INSTAAR at the University of Colorado Boulder (to J. Sepúlveda), the European Research Council (Hades-
794 ERC, grant agreement number 669947, to R.N. Glud), and the Max Planck Society. EF was also partially
795 supported by the UCO 1866 Student Scholarship-2019, Directorate of Graduate Studies, Universidad of
796 Concepción. We are thankful to the captains, crews, and scientists of the German RV *Sonne* cruises SO-261
797 (HADES-ERC) and SO-211 (ChiMeBo). In particular, we thank the chief scientists R.N. Glud and F. Wenzhöfer
798 (HADES-ERC) and D. Hebbeln (ChiMeBo). The HADES-ERC and ChiMeBo cruises were funded by the
799 European Research Council and the German Bundesministerium für Bildung & Forschung (BMBF),
800 respectively. We also wish to thank Carina Lange and Silvio Pantoja for access to samples from the ChiMeBo
801 cruise and M. Pizarro-Koch for the preparation of the three-dimensional map. We also thank L. Nuñez, B. Srain,
802 R. Castro, A. Ávila, M. Mohtadi, R. De Pol-Holz, and G. Martínez-Méndez, for sample collection during the
803 ChiMeBo cruise and/or laboratory assistance.

804

805 **References**

806

807 Ahumada, R.: Producción y destino de la biomasa fitoplanctónica en un sistema de bahías en Chile central: una
808 hipótesis, Biol PesqChile, 18, 53–66, 1989.

809 Allemann, M. N. and Allen, E. E.: Genetic suppression of lethal mutations in fatty acid biosynthesis mediated by
810 a secondary lipid synthase, Appl. Environ. Microbiol., 87, 2021.

811

812 Allen, E. E., Facciotti, D., and Bartlett, D. H.: Monounsaturated but not polyunsaturated fatty acids are required
813 for growth of the deep-sea bacterium *Photobacterium profundum* SS9 at high pressure and low temperature, Appl.
814 Environ. Microbiol., 65, 1710–1720, 1999.

815 Angel, M.: Detrital organic fluxes through pelagic ecosystems, in: Flows of energy and materials in marine
816 ecosystems, Springer, 475–516, 1984.

817 Angel, M. V.: Ocean trench conservation, *Environmentalist*, 2, 1–17, 1982.

818 Araki, S., Eichenberger, W., Sakurai, T., and Sato, N.: Distribution of diacylglycerylhydroxymethyltrimethyl- β -alanine (DGTA) and phosphatidylcholine in brown algae, *Plant Cell Physiol.*, 32, 623–628, 1991.

820 Baird, B.: Biomass and community structure of the abyssal microbiota determined from basin and Puerto Rico trench sediments, *Benthic Ecol. Sediment. Process. Venezuela Basin-Past Present*, 61, 217–213, 1985.

822 Bao, R., Strasser, M., McNichol, A. P., Haghipour, N., McIntyre, C., Wefer, G., and Eglington, T. I.: Tectonically-triggered sediment and carbon export to the Hadal zone, *Nat. Commun.*, 9, 1–8, 2018.

824 Barridge, J. K. and Shively, J.: Phospholipids of the Thiobacilli, *J. Bacteriol.*, 95, 2182–2185, 1968.

825 Batrakov, S. G. and Nikitin, D. I.: Lipid composition of the phosphatidylcholine-producing bacterium *Hyphomicrobium vulgare* NP-160, *Biochim. Biophys. Acta BBA-Lipids Lipid Metab.*, 1302, 129–137, 1996.

827 Benning, C., Huang, Z.-H., and Gage, D. A.: Accumulation of a novel glycolipid and a betaine lipid in cells of *Rhodobacter sphaeroides* grown under phosphate limitation, *Arch. Biochem. Biophys.*, 317, 103–111, 1995.

829 Bergé, J.-P. and Barnathan, G.: Fatty acids from lipids of marine organisms: molecular biodiversity, roles as biomarkers, biologically active compounds, and economical aspects, *Mar. Biotechnol. I*, 49–125, 2005.

831 Biddle, J. F., Lipp, J. S., Lever, M. A., Lloyd, K. G., Sørensen, K. B., Anderson, R., Fredricks, H. F., Elvert, M., Kelly, T. J., Schrag, D. P., and others: Heterotrophic Archaea dominate sedimentary subsurface ecosystems off Peru, *Proc. Natl. Acad. Sci.*, 103, 3846–3851, 2006.

834 Billett, D., Lampitt, R., Rice, A., and Mantoura, R.: Seasonal sedimentation of phytoplankton to the deep-sea benthos, *Nature*, 302, 520–522, 1983.

836 Bligh, E. G. and Dyer, W. J.: A rapid method of total lipid extraction and purification, *Can. J. Biochem. Physiol.*, 37, 911–917, 1959.

838 Boyer, G. M., Schubotz, F., Summons, R. E., Woods, J., and Shock, E. L.: Carbon oxidation state in microbial polar lipids suggests adaptation to hot spring temperature and redox gradients, *Front. Microbiol.*, 11, 229, 2020.

840 Brandsma, J., Hopmans, E., Philippart, C., Veldhuis, M., Schouten, S., and Damsté, J. S.: Temporal variations in abundance and composition of intact polar lipids in North Sea coastal marine water, *Biogeosciences Discuss.*, 8, 8895, 2011.

843 Brandsma, J., Hopmans, E., Philippart, C., Veldhuis, M., Schouten, S., and Sinninghe Damsté, J.: Low temporal variation in the intact polar lipid composition of North Sea coastal marine water reveals limited chemotaxonomic value, *Biogeosciences*, 9, 1073–1084, 2012.

846 Bühring, S. I., Kamp, A., Wörmer, L., Ho, S., and Hinrichs, K.-U.: Functional structure of laminated microbial
847 sediments from a supratidal sandy beach of the German Wadden Sea (St. Peter-Ording), *J. Sea Res.*, 85, 463–473,
848 2014.

849 Cañavate, J. P., Armada, I., and Hachero-Cruzado, I.: Interspecific variability in phosphorus-induced lipid
850 remodelling among marine eukaryotic phytoplankton, *New Phytol.*, 213, 700–713, 2017.

851 Cantarero, S. I., Henríquez-Castillo, C., Dildar, N., Vargas, C. A., Von Dassow, P., Cornejo-D’Ottone, M., and
852 Sepúlveda, J.: Size-fractionated contribution of microbial biomass to suspended organic matter in the eastern
853 Tropical South Pacific oxygen minimum zone, *Front. Mar. Sci.*, 7, 745, 2020.

854 Carini, P., Van Mooy, B. A., Thrash, J. C., White, A., Zhao, Y., Campbell, E. O., Fredricks, H. F., and Giovannoni,
855 S. J.: SAR11 lipid renovation in response to phosphate starvation, *Proc. Natl. Acad. Sci.*, 112, 7767–7772, 2015.

856 Clarke, K. and Gorley, R.: Getting started with PRIMER v7, *Primer-E Plymouth Plymouth Mar. Lab.*, 20, 2015.

857 da Costa, E., Amaro, H. M., Melo, T., Guedes, A. C., and Domingues, M. R.: Screening for polar lipids,
858 antioxidant, and anti-inflammatory activities of *Gloeothece* sp. lipid extracts pursuing new phytochemicals from
859 cyanobacteria, *J. Appl. Phycol.*, 32, 3015–3030, 2020.

860 Danovaro, R., Della Croce, N., Dell’Anno, A., and Pusceddu, A.: A depocenter of organic matter at 7800 m depth
861 in the SE Pacific Ocean, *Deep Sea Res. Part Oceanogr. Res. Pap.*, 50, 1411–1420, 2003.

862 Danovaro, R., Snelgrove, P. V., and Tyler, P.: Challenging the paradigms of deep-sea ecology, *Trends Ecol. Evol.*,
863 29, 465–475, 2014.

864 DeLong, E. F. and Yayanos, A. A.: Adaptation of the membrane lipids of a deep-sea bacterium to changes in
865 hydrostatic pressure, *Science*, 228, 1101–1103, 1985.

866 Dembitsky, V. M.: Betaine ether-linked glycerolipids: chemistry and biology, *Prog. Lipid Res.*, 35, 1–51, 1996.

867 Dowhan, W.: Molecular basis for membrane phospholipid diversity: why are there so many lipids?, *Annu. Rev.*
868 *Biochem.*, 66, 199–232, 1997.

869 Eichenberger, W. and Gribi, C.: Lipids of *Pavlova lutheri*: cellular site and metabolic role of DGCC,
870 *Phytochemistry*, 45, 1561–1567, 1997.

871 Eloe, E. A., Shulse, C. N., Fadrosh, D. W., Williamson, S. J., Allen, E. E., and Bartlett, D. H.: Compositional
872 differences in particle-associated and free-living microbial assemblages from an extreme deep-ocean
873 environment, *Environ. Microbiol. Rep.*, 3, 449–458, 2011.

874 Fang, J., Barcelona, M. J., Nogi, Y., and Kato, C.: Biochemical implications and geochemical significance of
875 novel phospholipids of the extremely barophilic bacteria from the Marianas Trench at 11,000 m, *Deep Sea Res.*
876 *Part Oceanogr. Res. Pap.*, 47, 1173–1182, 2000.

877 Fernández-Urruzola, I., Ulloa, O., Glud, R., Pinkerton, M., Schneider W., Wenzhöfer, F. and Escribano, R:
878 Plankton respiration in the Atacama Trench region: Implications for particulate organic carbon fux into the hadal
879 realm, *Limnol. Oceanogr.*, 2021.

880 Fischer, J. P., Ferdelman, T. G., D'Hondt, S., Røy, H., and Wenzhöfer, F.: Oxygen penetration deep into the
881 sediment of the South Pacific gyre, *Biogeosciences*, 6, 1467–1478, 2009.

882 Gao, Y., Du, X. Xu, W., Fan, R., Zhang, X., Yang, S., Chen, X., Lv, J., Luo, Z. Fungal diversity in deep sea
883 sediments from east yap trench and their denitrification potential. *Geomicrobiol. J.*, 1–11, 2020.

884 Gašparović, B., Penezić, A., Frka, S., Kazazić, S., Lampitt, R. S., Holguin, F. O., Sudasinghe, N., and Schaub, T.:
885 Particulate sulfur-containing lipids: Production and cycling from the epipelagic to the abyssopelagic zone, *Deep
886 Sea Res. Part Oceanogr. Res. Pap.*, 134, 12–22, 2018.

887 Geiger, O., Röhrs, V., Weissenmayer, B., Finan, T. M., and Thomas-Oates, J. E.: The regulator gene *phoB*
888 mediates phosphate stress-controlled synthesis of the membrane lipid diacylglycerol-N, N, N-
889 trimethylhomoserine in *Rhizobium (Sinorhizobium) meliloti*, *Mol. Microbiol.*, 32, 63–73, 1999.

890 Glud, R. N., Wenzhöfer, F., Middelboe, M., Oguri, K., Turnewitsch, R., Canfield, D. E., and Kitazato, H.: High
891 rates of microbial carbon turnover in sediments in the deepest oceanic trench on Earth, *Nat. Geosci.*, 6, 284–288,
892 2013.

893 Glud, R. N., Berg, P., Thamdrup, B., Larsen, M., Stewart, H. A., Jamieson, A. J., Glud, A., Oguri, K., Sanei, H.,
894 Rowden, A. A., and others: Hadal trenches are dynamic hotspots for early diagenesis in the deep sea, *Commun.
895 Earth Environ.*, 2, 1–8, 2021.

896 Goldfine, H.: Bacterial membranes and lipid packing theory, *J. Lipid Res.*, 25, 1501–1507, 1984.

897 Goldfine, H. and Hagen, P.-O.: N-Methyl groups in bacterial lipids III. phospholipids of hyphomicrobia, *J.
898 Bacteriol.*, 95, 367–375, 1968.

899 Gombos, Z., Várkonyi, Z., Hagio, M., Iwaki, M., Kovács, L., Masamoto, K., Itoh, S., and Wada, H.:
900 Phosphatidylglycerol requirement for the function of electron acceptor plastoquinone QB in the photosystem II
901 reaction center, *Biochemistry*, 41, 3796–3802, 2002.

902 Gómez-Consarnau, L., González, J. M., Coll-Lladó, M., Gourdon, P., Pascher, T., Neutze, R., Pedrós-Alió, C.,
903 and Pinhassi, J.: Light stimulates growth of proteorhodopsin-containing marine Flavobacteria, *Nature*, 445, 210–
904 213, 2007.

905 Gooday, A. J., Bett, B. J., Escobar, E., Ingole, B., Levin, L. A., Neira, C., Raman, A. V., and Sellanes, J.: Habitat
906 heterogeneity and its influence on benthic biodiversity in oxygen minimum zones, *Mar. Ecol.*, 31, 125–147, 2010.

907 Gounaris, K. and Barber, J.: Monogalactosyldiacylglycerol: the most abundant polar lipid in nature, *Trends
908 Biochem. Sci.*, 8, 378–381, 1983.

909 Gutiérrez, M. H., Vera J., Srain B., Quiñones, R. A., Wörmer L., Hinrichs K.-U., and Pantoja, S. Biochemical
910 fingerprints of marine fungi: implications for trophic and biogeochemical studies. *Aquat. Microb. Ecol.*, 2020.

911 Guan, H., Chen, L., Luo, M., Liu, L., Mao, S., Ge, H., Zhang, M., Fang, J., and Chen, D.: Composition and origin
912 of lipid biomarkers in the surface sediments from the southern Challenger Deep, Mariana Trench, *Geosci. Front.*,
913 10, 351–360, 2019.

914 Grabowski, E., Letelier, R. M., Laws, E. A., and Karl, D. M.: Coupling carbon and energy fluxes in the North
915 Pacific Subtropical Gyre, *Nat. Commun.*, 10, 1895, 2019.

916 Hand, K., Bartlett, D., Fryer, P., Peoples, L., Williford, K., Hofmann, A., and Cameron, J.: Discovery of novel
917 structures at 10.7 km depth in the Mariana Trench may reveal chemolithoautotrophic microbial communities,
918 *Deep Sea Res. Part Oceanogr. Res. Pap.*, 160, 103238, 2020.

919 Harvey, H. R., Fallon, R. D., and Patton, J. S.: The effect of organic matter and oxygen on the degradation of
920 bacterial membrane lipids in marine sediments, *Geochim. Cosmochim. Acta*, 50, 795–804, 1986.

921 Harwood, J. L.: Membrane lipids in algae, in: *Lipids in photosynthesis: structure, function and genetics*, Springer,
922 53–64, 1998.

923 Hedges, J. I., Baldock, J. A., Gélinas, Y., Lee, C., Peterson, M., and Wakeham, S. G.: Evidence for non-selective
924 preservation of organic matter in sinking marine particles, *Nature*, 409, 801–804, 2001.

925 Heinz, E.: Enzymatic reactions in galactolipid biosynthesis, in: *Lipids and lipid polymers in higher plants*,
926 Springer, 102–120, 1977.

927 Hiraoka, S., Hirai, M., Matsui, Y., Makabe, A., Minegishi, H., Tsuda, M., Rastelli, E., Danovaro, R., Corinaldesi,
928 C., Kitahashi, T., and others: Microbial community and geochemical analyses of trans-trench sediments for
929 understanding the roles of hadal environments, *ISME J.*, 14, 740–756, 2020.

930 Houston, J.: Variability of precipitation in the Atacama Desert: its causes and hydrological impact, *Int. J. Climatol.*
931 *J. R. Meteorol. Soc.*, 26, 2181–2198, 2006.

932 Hunter, J. E.: Phytoplankton lipidomics: lipid dynamics in response to microalgal stressors, PhD Thesis,
933 University of Southampton, 2015.

934 Ichino, M. C., Clark, M. R., Drazen, J. C., Jamieson, A., Jones, D. O., Martin, A. P., Rowden, A. A., Shank, T.
935 M., Yancey, P. H., and Ruhl, H. A.: The distribution of benthic biomass in hadal trenches: a modelling approach
936 to investigate the effect of vertical and lateral organic matter transport to the seafloor, *Deep Sea Res. Part*
937 *Oceanogr. Res. Pap.*, 100, 21–33, 2015.

938 Imhoff, J. F.: Taxonomy and physiology of phototrophic purple bacteria and green sulfur bacteria, in: *Anoxygenic*
939 *photosynthetic bacteria*, Springer, 1–15, 1995.

940 Inthorn, M., Wagner, T., Scheeder, G., and Zabel, M.: Lateral transport controls distribution, quality, and burial
941 of organic matter along continental slopes in high-productivity areas, *Geology*, 34, 205–208, 2006.

942 Itoh, M., Kawamura, K., Kitahashi, T., Kojima, S., Katagiri, H., and Shimanaga, M.: Bathymetric patterns of
943 meiofaunal abundance and biomass associated with the Kuril and Ryukyu trenches, western North Pacific Ocean,
944 *Deep Sea Res. Part Oceanogr. Res. Pap.*, 58, 86–97, 2011.

945 Itou, M., Matsumura, I., and Noriki, S.: A large flux of particulate matter in the deep Japan Trench observed just
946 after the 1994 Sanriku-Oki earthquake, *Deep Sea Res. Part Oceanogr. Res. Pap.*, 47, 1987–1998, 2000.

947 Jahnke, R. A. and Jahnke, D. B.: Rates of C, N, P and Si recycling and denitrification at the US Mid-Atlantic
948 continental slope depocenter, *Deep Sea Res. Part Oceanogr. Res. Pap.*, 47, 1405–1428, 2000.

949 Jahnke, R. A., Reimers, C. E., and Craven, D. B.: Intensification of recycling of organic matter at the sea floor
950 near ocean margins, *Nature*, 348, 50–54, 1990.

951 Jamieson, A. J., Fujii, T., Mayor, D. J., Solan, M., and Priede, I. G.: Hadal trenches: the ecology of the deepest
952 places on Earth, *Trends Ecol. Evol.*, 25, 190–197, 2010.

953 Jebbar, M., Franzetti, B., Girard, E., and Oger, P.: Microbial diversity and adaptation to high hydrostatic pressure
954 in deep-sea hydrothermal vents prokaryotes, *Extremophiles*, 19, 721–740, 2015.

955

956 Kalisch, B., Dörmann, P., and Hözl, G.: DGDG and glycolipids in plants and algae, *Lipids Plant Algae Dev.*, 51–
957 83, 2016.

958 Kaneda, T.: Iso-and anteiso-fatty acids in bacteria: biosynthesis, function, and taxonomic significance., *Microbiol.*
959 *Mol. Biol. Rev.*, 55, 288–302, 1991.

960 Kato, C., Masui, N., and Horikoshi, K.: Properties of obligately barophilic bacteria isolated from a sample of
961 deep-sea sediment from the Izu-Bonin trench, *Oceanogr. Lit. Rev.*, 1, 53–54, 1997.

962 Kato, M., Adachi, K., Hajiro-Nakanishi, K., Ishigaki, E., Sano, H., and Miyachi, S.: betaine lipid from *Pavolova*
963 *lutheri*, *Phytochemistry*, 1994.

964 Kioka, A., Schwestermann, T., Moernaut, J., Ikehara, K., Kanamatsu, T., Eglinton, T. I., and Strasser, M.: Event
965 stratigraphy in a hadal oceanic trench: The Japan trench as sedimentary archive recording recurrent giant
966 subduction zone earthquakes and their role in organic carbon export to the deep sea, *Front. Earth Sci.*, 7, 319,
967 2019.

968 Kobližek, M., Falkowski, P. G., and Kolber, Z. S.: Diversity and distribution of photosynthetic bacteria in the
969 Black Sea, *Deep Sea Res. Part II Top. Stud. Oceanogr.*, 53, 1934–1944, 2006.

970 Koga, Y. and Morii, H.: Biosynthesis of ether-type polar lipids in archaea and evolutionary considerations,
971 *Microbiol. Mol. Biol. Rev.*, 71, 97–120, 2007.

972 Komatsu, H. and Chong, P. L.-G.: Low permeability of liposomal membranes composed of bipolar tetraether
973 lipids from thermoacidophilic archaeabacterium *Sulfolobus acidocaldarius*, *Biochemistry*, 37, 107–115, 1998.

974 Lam, P., Jensen, M. M., Lavik, G., McGinnis, D. F., Müller, B., Schubert, C. J., Amann, R., Thamdrup, B., and
975 Kuypers, M. M.: Linking crenarchaeal and bacterial nitrification to anammox in the Black Sea, *Proc. Natl. Acad.*
976 *Sci.*, 104, 7104–7109, 2007.

977 Lechevalier, H.: Chemotaxonomic use of lipids—an overview, *Microb. Lipids*, 1, 869–902, 1988.

978 Leduc, D., Rowden, A. A., Glud, R. N., Wenzhöfer, F., Kitazato, H., and Clark, M. R.: Comparison between
979 infaunal communities of the deep floor and edge of the Tonga Trench: possible effects of differences in organic
980 matter supply, *Deep Sea Res. Part Oceanogr. Res. Pap.*, 116, 264–275, 2016.

981 Lipp, J. S. and Hinrichs, K.-U.: Structural diversity and fate of intact polar lipids in marine sediments, *Geochim.*
982 *Cosmochim. Acta*, 73, 6816–6833, 2009a.

983 Lipp, J. S. and Hinrichs, K.-U.: Structural diversity and fate of intact polar lipids in marine sediments, *Geochim.*
984 *Cosmochim. Acta*, 73, 6816–6833, 2009b.

985 Lipp, J. S., Morono, Y., Inagaki, F., and Hinrichs, K.-U.: Significant contribution of Archaea to extant biomass in
986 marine subsurface sediments, *Nature*, 454, 991–994, 2008.

987 Liu, J., Zheng, Y., Lin, H., Wang, X., Li, M., Liu, Y., Yu, M., Zhao, M., Pedentchouk, N., Lea-Smith, D. J., and
988 others: Proliferation of hydrocarbon-degrading microbes at the bottom of the Mariana Trench, *Microbiome*, 7, 1–
989 13, 2019.

990 Liu, X., Lipp, J. S., and Hinrichs, K.-U.: Distribution of intact and core GDGTs in marine sediments, *Org.*
991 *Geochem.*, 42, 368–375, 2011.

992 Liu, X.-L., Lipp, J. S., Simpson, J. H., Lin, Y.-S., Summons, R. E., and Hinrichs, K.-U.: Mono-and dihydroxyl
993 glycerol dibiphytanyl glycerol tetraethers in marine sediments: Identification of both core and intact polar lipid
994 forms, *Geochim. Cosmochim. Acta*, 89, 102–115, 2012.

995 Logemann, J., Graue, J., Köster, J., Engelen, B., Rullkötter, J., and Cypionka, H.: A laboratory experiment of
996 intact polar lipid degradation in sandy sediments, *Biogeosciences*, 8, 2547–2560, 2011.

997 López-Lara, I. M., Sohlenkamp, C., and Geiger, O.: Membrane lipids in plant-associated bacteria: their
998 biosyntheses and possible functions, *Mol. Plant. Microbe Interact.*, 16, 567–579, 2003.

999 Lund, E. D. and Chu, F.-L. E.: Phospholipid biosynthesis in the oyster protozoan parasite, *Perkinsus marinus*,
1000 *Mol. Biochem. Parasitol.*, 121, 245–253, 2002.

1001 Luo, M., Gieskes, J., Chen, L., Shi, X., and Chen, D.: Provenances, distribution, and accumulation of organic
1002 matter in the southern Mariana Trench rim and slope: Implication for carbon cycle and burial in hadal trenches,
1003 *Mar. Geol.*, 386, 98–106, 2017.

1004 Macdonald, A.: The effects of pressure on the molecular structure and physiological functions of cell membranes,
1005 *Philos. Trans. R. Soc. Lond. B Biol. Sci.*, 304, 47–68, 1984.

1006 Makula, R.: Phospholipid composition of methane-utilizing bacteria., *J. Bacteriol.*, 134, 771–777, 1978.

1007 Mangelsdorf, K., Zink, K.-G., Birrien, J.-L., and Toffin, L.: A quantitative assessment of pressure dependent
1008 adaptive changes in the membrane lipids of a piezosensitive deep sub-seafloor bacterium, *Org. Geochem.*, 36,
1009 1459–1479, 2005.

1010 Martin, J. H., Knauer, G. A., Karl, D. M., and Broenkow, W. W.: VERTEX: carbon cycling in the northeast
1011 Pacific, *Deep Sea Res. Part Oceanogr. Res. Pap.*, 34, 267–285, 1987.

1012 Matys, E., Sepúlveda, J., Pantoja, S., Lange, C., Caniupán, M., Lamy, F., and Summons, R. E.:
1013 Bacteriohopanepolyols along redox gradients in the Humboldt Current System off northern Chile, *Geobiology*,
1014 15, 844–857, 2017.

1015 Mayzaud, P., Virtue, P., and Albessard, E.: Seasonal variations in the lipid and fatty acid composition of the
1016 euphausiid *Meganyctiphanes norvegica* from the Ligurian Sea, *Mar. Ecol. Prog. Ser.*, 186, 199–210, 1999.

1017 Mirzaei, A., Rahmati, M., and Ahmadi, M.: A new method for hierarchical clustering combination, *Intell. Data
1018 Anal.*, 12, 549–571, 2008.

1019 Murata, N. and Siegenthaler, P.-A.: Lipids in photosynthesis: an overview, *Lipids Photosynth. Struct. Funct.
1020 Genet.*, 1–20, 1998.

1021 Morii, H., Ogawa, M., Fukuda, K. and Taniguchi, H. Ubiquitous distribution of phosphatidylinositol phosphate
1022 synthase and archaetidylinositol phosphate synthase in Bacteria and Archaea, which contain inositol phospholipid,
1023 *Biochem. Bioph. Res*, 275, 36568–36574, 2014.

1024 Nichols, D. S., Miller, M. R., Davies, N. W., Goodchild, A., Raftery, M., and Cavicchioli, R.: Cold adaptation in
1025 the Antarctic archaeon *Methanococcoides burtonii* involves membrane lipid unsaturation, *J. Bacteriol.*, 186,
1026 8508–8515, 2004.

1027 Nunoura, T., Takaki, Y., Hirai, M., Shimamura, S., Makabe, A., Koide, O., Kikuchi, T., Miyazaki, J., Koba, K.,
1028 Yoshida, N., and others: Hadal biosphere: insight into the microbial ecosystem in the deepest ocean on Earth,
1029 *Proc. Natl. Acad. Sci.*, 112, E1230–E1236, 2015.

1030 Nunoura, T., Hirai, M., Yoshida-Takashima, Y., Nishizawa, M., Kawagucci, S., Yokokawa, T., Miyazaki, J.,
1031 Koide, O., Makita, H., Takaki, Y., and others: Distribution and niche separation of planktonic microbial
1032 communities in the water columns from the surface to the hadal waters of the Japan Trench under the Eutrophic
1033 Ocean, *Front. Microbiol.*, 7, 1261, 2016.

1034 Nunoura, T., Nishizawa, M., Hirai, M., Shimamura, S., Harnvoravongchai P., Koide, O., Morono, Y., Fukui, T.,
1035 Inagaki, F., Miyazaki, J., Takaki, Y., and others: Microbial Diversity in Sediments from the Bottom of the
1036 Challenger Deep, the Mariana Trench, *Microbes Environ.*, 33, 186–194, 2018.

1037 Oksanen, J., Blanchet, F. G., Kindt, R., Legendre, P., Minchin, P., O'hara, R., Simpson, G., Solymos, P., Stevens,
1038 M., Wagner, H., and others: Community ecology package, R Package Version, 2, 2013.

1039 Oliver, J. D. and Colwell, R. R.: Extractable lipids of gram-negative marine bacteria: phospholipid composition,
1040 *J. Bacteriol.*, 114, 897–908, 1973.

1041 Patton, S., Lee, R. F., and Benson, A. A.: The presence of unusually high levels of lysophosphatidylethanolamine
1042 in a wax ester-synthesizing copepod (*Calanus plumchrus*), *Biochim. Biophys. Acta BBA-Lipids Lipid Metab.*,
1043 270, 479–488, 1972.

1044 Periasamy, N., Teichert, H., Weise, K., Vogel, R. F., and Winter, R.: Effects of temperature and pressure on the
1045 lateral organization of model membranes with functionally reconstituted multidrug transporter LmrA, *Biochim.*
1046 *Biophys. Acta BBA-Biomembr.*, 1788, 390–401, 2009.

1047

1048 Petersen, S. O., Henriksen, K., Blackburn, T. H., and King, G. M.: A comparison of phospholipid and chloroform
1049 fumigation analyses for biomass in soil: potentials and limitations, *FEMS Microbiol. Lett.*, 85, 257–267, 1991.

1050 Pitcher, A. M.: Intact polar lipids of ammonia-oxidizing Archaea: structural diversity application in molecular
1051 ecology, PhD Thesis, Departement Aardwetenschappen, 2011.

1052 Poff, K. E., Leu, A. O., Eppley, J. M., Karl, D. M., and DeLong, E. F.: Microbial dynamics of elevated carbon
1053 flux in the open ocean's abyss, *Proc. Natl. Acad. Sci.*, 118, 2021.

1054 Pond, D. and Harris, R.: The lipid composition of the coccolithophore *Emiliania huxleyi* and its possible
1055 ecophysiological significance, *J. Mar. Biol. Assoc. U. K.*, 76, 579–594, 1996.

1056 Popendorf, K., Tanaka, T., Pujo-Pay, M., Lagaria, A., Courties, C., Conan, P., Oriol, L., Sofen, L., Moutin, T.,
1057 and Van Mooy, B. A.: Gradients in intact polar diacylglycerolipids across the Mediterranean Sea are related to
1058 phosphate availability, *Biogeosciences*, 8, 3733–3745, 2011a.

1059 Popendorf, K. J., Lomas, M. W., and Van Mooy, B. A.: Microbial sources of intact polar diacylglycerolipids in
1060 the Western North Atlantic Ocean, *Org. Geochem.*, 42, 803–811, 2011b.

1061 Ratledge, C. and Wilkinson, S. G.: *Microbial lipids*, Academic press, 1988.

1062 Rex, M. A., Etter, R. J., Morris, J. S., Crouse, J., McClain, C. R., Johnson, N. A., Stuart, C. T., Deming, J. W.,
1063 Thies, R., and Avery, R.: Global bathymetric patterns of standing stock and body size in the deep-sea benthos,
1064 *Mar. Ecol. Prog. Ser.*, 317, 1–8, 2006.

1065 Řezanka, T. and Sigler, K.: Odd-numbered very-long-chain fatty acids from the microbial, animal and plant
1066 kingdoms, *Prog. Lipid Res.*, 48, 206–238, 2009.

1067 Řezanka, T., Viden, I., Go, J., Dor, I., and Dembitsky, V.: Polar lipids and fatty acids of three wild cyanobacterial
1068 strains of the genus *Chroococcidiopsis*, *Folia Microbiol. (Praha)*, 48, 781–786, 2003.

1069 Rossel, P. E., Elvert, M., Ramette, A., Boetius, A., and Hinrichs, K.-U.: Factors controlling the distribution of
1070 anaerobic methanotrophic communities in marine environments: evidence from intact polar membrane lipids,
1071 *Geochim. Cosmochim. Acta*, 75, 164–184, 2011.

1072 Rütters, H., Sass, H., Cypionka, H., and Rullkötter, J.: Monoalkylether phospholipids in the sulfate-reducing
1073 bacteria *Desulfosarcina variabilis* and *Desulforhabdus amnigenus*, *Arch. Microbiol.*, 176, 435–442, 2001.

1074 Sabbatini, A., Morigi, C., Negri, A., and Gooday, A. J.: Soft-shelled benthic foraminifera from a hadal site (7800
1075 m water depth) in the Atacama Trench (SE Pacific): preliminary observations, *J. Micropalaeontology*, 21, 131–
1076 135, 2002.

1077 Sakurai, I., Shen, J.-R., Leng, J., Ohashi, S., Kobayashi, M., and Wada, H.: Lipids in oxygen-evolving
1078 photosystem II complexes of cyanobacteria and higher plants, *J. Biochem. (Tokyo)*, 140, 201–209, 2006.

1079 Sato, N.: Betaine lipids, *Bot. Mag. Shokubutsu-Gaku-Zasshi*, 105, 185–197, 1992.

1080 Sato, N., Hagio, M., Wada, H., and Tsuzuki, M.: Requirement of phosphatidylglycerol for photosynthetic function
1081 in thylakoid membranes, *Proc. Natl. Acad. Sci.*, 97, 10655–10660, 2000.

1082 Schauberger, C., Middelboe, M., Larsen, M., Peoples, L. M., Bartlett, D. H., Kirpekar, F., Rowden, A. A.,
1083 Wenzhöfer, F., Thamdrup, B., and Glud, R. N.: Spatial variability of prokaryotic and viral abundances in the
1084 Kermadec and Atacama Trench regions, *Limnol. Oceanogr.*, 2021.

1085 Schneider, W., Fuenzalida, R., Garcés-Vargas, J., Bravo, L., and Lange, C.: Extensión vertical y horizontal de la
1086 zona de mínima oxígeno en el Pacífico Sur Oriental, *Gayana Concepc.*, 70, 79–82, 2006.

1087 Schouten, S., Middelburg, J. J., Hopmans, E. C., and Damsté, J. S. S.: Fossilization and degradation of intact polar
1088 lipids in deep subsurface sediments: a theoretical approach, *Geochim. Cosmochim. Acta*, 74, 3806–3814, 2010.

1089 Schubotz, F., Wakeham, S. G., Lipp, J. S., Fredricks, H. F., and Hinrichs, K.-U.: Detection of microbial biomass
1090 by intact polar membrane lipid analysis in the water column and surface sediments of the Black Sea, *Environ.*
1091 *Microbiol.*, 11, 2720–2734, 2009a.

1092 Schubotz, F., Wakeham, S. G., Lipp, J. S., Fredricks, H. F., and Hinrichs, K.-U.: Detection of microbial biomass
1093 by intact polar membrane lipid analysis in the water column and surface sediments of the Black Sea, *Environ.*
1094 *Microbiol.*, 11, 2720–2734, 2009b.

1095 Schubotz, F., Meyer-Dombard, D., Bradley, A. S., Fredricks, H. F., Hinrichs, K.-U., Shock, E., and Summons, R.
1096 E.: Spatial and temporal variability of biomarkers and microbial diversity reveal metabolic and community
1097 flexibility in Streamer Biofilm Communities in the Lower Geyser Basin, *Yellowstone National Park, Geobiology*,
1098 11, 549–569, 2013.

1099 Schubotz, F., Xie, S., Lipp, J. S., Hinrichs, K.-U., and Wakeham, S. G.: Intact polar lipids in the water column of
1100 the eastern tropical North Pacific: abundance and structural variety of non-phosphorus lipids, *Biogeosciences*, 15,
1101 6481–6501, 2018a.

1102 Schwestermann, T., Eglinton, T., Haghipour, N., McNichol, A., Ikebara, K., and Strasser, M.: Event-dominated
1103 transport, provenance, and burial of organic carbon in the Japan Trench, *Earth Planet. Sci. Lett.*, 563, 116870,
1104 2021.

1105 Sebastián, M., Smith, A. F., González, J. M., Fredricks, H. F., Van Mooy, B., Koblížek, M., Brandsma, J., Koster,
1106 G., Mestre, M., Mostajir, B., and others: Lipid remodelling is a widespread strategy in marine heterotrophic
1107 bacteria upon phosphorus deficiency, *ISME J.*, 10, 968–978, 2016.

1108 Shaw, N.: Lipid composition as a guide to the classification of bacteria, *Adv. Appl. Microbiol.*, 17, 63–108, 1974.

1109 Siegenthaler, P.-A.: Molecular organization of acyl lipids in photosynthetic membranes of higher plants, in: *Lipids*
1110 in photosynthesis: structure, function and genetics, Springer, 119–144, 1998.

1111 Siliakus, M. F., van der Oost, J., and Kengen, S. W.: Adaptations of archaeal and bacterial membranes to variations
1112 in temperature, pH and pressure, *Extremophiles*, 21, 651–670, 2017.

1113 Smith, C.: Chemosynthesis in the deep-sea: life without the sun, *Biogeosciences Discuss.*, 9, 17037–17052, 2012.

1114 Sohlenkamp, C., López-Lara, I. M., and Geiger, O.: Biosynthesis of phosphatidylcholine in bacteria, *Prog. Lipid*
1115 *Res.*, 42, 115–162, 2003.

1116 Somero, G. N.: Adaptations to high hydrostatic pressure., *Annu. Rev. Physiol.*, 54, 557–577, 1992.

1117 Stockton, W. L. and DeLaca, T. E.: Food falls in the deep sea: occurrence, quality, and significance, *Deep Sea*
1118 *Res. Part Oceanogr. Res. Pap.*, 29, 157–169, 1982.

1119 Sturt, H. F., Summons, R. E., Smith, K., Elvert, M., and Hinrichs, K.-U.: Intact polar membrane lipids in
1120 prokaryotes and sediments deciphered by high-performance liquid chromatography/electrospray ionization
1121 multistage mass spectrometry—new biomarkers for biogeochemistry and microbial ecology, *Rapid Commun.*
1122 *Mass Spectrom.*, 18, 617–628, 2004.

1123 Suzuki, R. and Shimodaira, H.: Pvclust: an R package for assessing the uncertainty in hierarchical clustering,
1124 *Bioinformatics*, 22, 1540–1542, 2006.

1125 Ta, K., Peng, X., Xu, H., Du, M., Chen, S., Li, J., and Zhang, C.: Distributions and sources of glycerol dialkyl
1126 glycerol tetraethers in sediment cores from the Mariana subduction zone, *J. Geophys. Res. Biogeosciences*, 124,
1127 857–869, 2019.

1128 Tamburini, C., Boutrif, M., Garel, M., Colwell, R. R., and Deming, J. W.: Prokaryotic responses to hydrostatic
1129 pressure in the ocean—a review, *Environ. Microbiol.*, 15, 1262–1274, 2013.

1130 Tarn, J., Peoples, L. M., Hardy, K., Cameron, J., and Bartlett, D. H.: Identification of free-living and particle-
1131 associated microbial communities present in hadal regions of the Mariana Trench, *Front. Microbiol.*, 7, 665, 2016.

1132 Thompson Jr, G. A.: Lipids and membrane function in green algae, *Biochim. Biophys. Acta BBA-Lipids Lipid*
1133 *Metab.*, 1302, 17–45, 1996.

1134 Turnewitsch, R., Falahat, S., Stehlikova, J., Oguri, K., Glud, R. N., Middelboe, M., Kitazato, H., Wenzhöfer, F.,
1135 Ando, K., Fujio, S., and others: Recent sediment dynamics in hadal trenches: evidence for the influence of higher-
1136 frequency (tidal, near-inertial) fluid dynamics, *Deep Sea Res. Part Oceanogr. Res. Pap.*, 90, 125–138, 2014.

1137 Van Mooy, B. A. and Fredricks, H. F.: Bacterial and eukaryotic intact polar lipids in the eastern subtropical South
1138 Pacific: water-column distribution, planktonic sources, and fatty acid composition, *Geochim. Cosmochim. Acta*,
1139 74, 6499–6516, 2010.

1140 Van Mooy, B. A., Rocap, G., Fredricks, H. F., Evans, C. T., and Devol, A. H.: Sulfolipids dramatically decrease
1141 phosphorus demand by picocyanobacteria in oligotrophic marine environments, *Proc. Natl. Acad. Sci.*, 103, 8607–
1142 8612, 2006.

1143 Van Mooy, B. A., Fredricks, H. F., Pedler, B. E., Dyhrman, S. T., Karl, D. M., Koblížek, M., Lomas, M. W.,
1144 Mincer, T. J., Moore, L. R., Moutin, T., and others: Phytoplankton in the ocean use non-phosphorus lipids in
1145 response to phosphorus scarcity, *Nature*, 458, 69–72, 2009.

1146 Vardi, A., Van Mooy, B. A., Fredricks, H. F., Popendorf, K. J., Ossolinski, J. E., Haramaty, L., and Bidle, K. D.:
1147 Viral glycosphingolipids induce lytic infection and cell death in marine phytoplankton, *Science*, 326, 861–865,
1148 2009.

1149 Vargas, C. A., Cantarero, S. I., Sepúlveda, J., Galán, A., De Pol-Holz, R., Walker, B., Schneider, W., Farías, L.,
1150 D’Ottone, M. C., Walker, J., and others: A source of isotopically light organic carbon in a low-pH anoxic marine
1151 zone, *Nat. Commun.*, 12, 1–11, 2021.

1152 Volkman, J., Jeffrey, S., Nichols, P., Rogers, G., and Garland, C.: Fatty acid and lipid composition of 10 species
1153 of microalgae used in mariculture, *J. Exp. Mar. Biol. Ecol.*, 128, 219–240, 1989.

1154 Wada, H. and Murata, N.: Membrane lipids in cyanobacteria, in: *Lipids in photosynthesis: structure, function and*
1155 *genetics*, Springer, 65–81, 1998.

1156 Wada, H. and Murata, N.: The essential role of phosphatidylglycerol in photosynthesis, *Photosynth. Res.*, 92,
1157 205–215, 2007.

1158 Wakeham, S. G., Lee, C., Farrington, J. W., and Gagosian, R. B.: Biogeochemistry of particulate organic matter
1159 in the oceans: results from sediment trap experiments, *Deep Sea Res. Part Oceanogr. Res. Pap.*, 31, 509–528,
1160 1984.

1161 Wakeham, S. G., Amann, R., Freeman, K. H., Hopmans, E. C., Jørgensen, B. B., Putnam, I. F., Schouten, S.,
1162 Damsté, J. S. S., Talbot, H. M., and Woebken, D.: Microbial ecology of the stratified water column of the Black
1163 Sea as revealed by a comprehensive biomarker study, *Org. Geochem.*, 38, 2070–2097, 2007.

1164 Wakeham, S. G., Turich, C., Schubotz, F., Podlaska, A., Li, X. N., Varela, R., Astor, Y., Saenz, J. P., Rush, D.,
1165 Damste, J. S. S., and others: Biomarkers, chemistry and microbiology show chemoautotrophy in a multilayer
1166 chemocline in the Cariaco Basin, *Deep Sea Res. Part Oceanogr. Res. Pap.*, 63, 133–156, 2012.

1167 Warnes, G., Bolker, B., Bonebakker, L., Gentleman, R., Liaw, W., Lumley, T., and others: gplots: various R
1168 programming tools for plotting data. R package version 2.16. 0. 2015, 2015.

1169 Warton, D. I., Wright, S. T., and Wang, Y.: Distance-based multivariate analyses confound location and dispersion
1170 effects, *Methods Ecol. Evol.*, 3, 89–101, 2012.

1171 Weijers, J. W., Schouten, S., van den Donker, J. C., Hopmans, E. C., and Damsté, J. S. S.: Environmental controls
1172 on bacterial tetraether membrane lipid distribution in soils, *Geochim. Cosmochim. Acta*, 71, 703–713, 2007.

1173 Wenzhöfer, F., Oguri, K., Middelboe, M., Turnewitsch, R., Toyofuku, T., Kitazato, H., and Glud, R. N.: Benthic
1174 carbon mineralization in hadal trenches: Assessment by in situ O₂ microprofile measurements, *Deep Sea Res.*
1175 *Part Oceanogr. Res. Pap.*, 116, 276–286, 2016.

1176 Wenzhöfer, F. The Expedition SO261 of the Research Vessel SONNE to the Atacama Trench in the Pacific Ocean
1177 in 2018. *Rep Polar Mar Res* 729:1–111. 2019.

1178 Westrich, J. T. and Berner, R. A.: The role of sedimentary organic matter in bacterial sulphate reduction – the G
1179 model tested, *Limnol. Oceanogr.*, 29, 236–249, 1984.

1180 White, D., Bobbie, R., King, J., Nickels, J., and Amoe, P.: Lipid analysis of sediments for microbial biomass and
1181 community structure, in: *Methodology for biomass determinations and microbial activities in sediments*, ASTM
1182 International, 1979.

1183 Winter, R.: Effect of lipid chain length, temperature, pressure and composition on the lateral organisation and
1184 phase behavior of lipid bilayer/gramicidin mixtures, in: *Biophysical Journal*, 153A-153A, 2002.

1185 Winter, R. and Jeworrek, C.: Effect of pressure on membranes, *Soft Matter*, 5, 3157–3173, 2009.

1186 Wörmer, L., Lipp, J. S., Schröder, J. M., and Hinrichs, K.-U.: Application of two new LC–ESI–MS methods for
1187 improved detection of intact polar lipids (IPLs) in environmental samples, *Org. Geochem.*, 59, 10–21, 2013.

1188 Xu, Y., Ge, H., and Fang, J.: Biogeochemistry of hadal trenches: Recent developments and future perspectives,
1189 *Deep Sea Res. Part II Top. Stud. Oceanogr.*, 155, 19–26, 2018.

1190 Xu, Y., Jia, Z., Xiao, W., Fang, J., Wang, Y., Luo, M., Wenzhöfer, F., Rowden, A. A., and Glud, R. N.: Glycerol
1191 dialkyl glycerol tetraethers in surface sediments from three Pacific trenches: Distribution, source and
1192 environmental implications, *Org. Geochem.*, 147, 104079, 2020.

1193 Xu, Y., Li, X., Luo, M., Xiao, W., Fang, J., Rashid, H., Peng, Y., Li, W., Wenzhöfer, F., Rowden, A. A., and
1194 others: Distribution, Source, and Burial of Sedimentary Organic Carbon in Kermadec and Atacama Trenches, *J.*
1195 *Geophys. Res. Biogeosciences*, 126, e2020JG006189, 2021.

1196 Yano, Y., Nakayama, A., Ishihara, K., and Saito, H.: Adaptive changes in membrane lipids of barophilic bacteria
1197 in response to changes in growth pressure, *Appl. Environ. Microbiol.*, 64, 479–485, 1998.

1198 Zhong, H., Lehtovirta-Morley, L., Liu, J., Zheng, Y., Lin, H., Song, D., Todd, J. D., Tian, J., and Zhang, X.-H.:
1199 Novel insights into the Thaumarchaeota in the deepest oceans: their metabolism and potential adaptation
1200 mechanisms, *Microbiome*, 8, 1–16, 2020.

1201 Zhukova, N. V.: Variation in microbial biomass and community structure in sediments of Peter the Great Bay
1202 (Sea of Japan/East Sea), as estimated from fatty acid biomarkers, *Ocean Sci. J.*, 40, 34–42, 2005.